catalysts

MDPI

Article

Sustainable Solar Mineralization of Polyvinylpyrrolidone via a Regenerable TiO_2/Cellulose–Activated Carbon Composite with Integrated Waste Reuse for Urea Oxidation

Samar M. Mahgoub [1], Hossain ABM Sharif [2], Ahmed A. Allam [2], Abdelatty M. Radalla [3], Hussein Nassar H. Eweis [3], Hala Mohamed [1] and Rehab Mahmoud [3,*]

[1] Materials Science and Nanotechnology Department, Faculty of Postgraduate Studies for Advanced Sciences, Beni-Suef University, Beni-Suef 62511, Egypt; miramar15@yahoo.com (S.M.M.); halamohamedpsas@yahoo.com (H.M.)
[2] Department of Biology, College of Science, Imam Mohammad Ibn Saud Islamic University (IMSIU), Riyadh 11623, Saudi Arabia; ashossain@imamu.edu.sa (H.A.S.); aallam@imamu.edu.sa (A.A.A.)
[3] Chemistry Department, Faculty of Science, Beni-Suef University, Beni-Suef 62511, Egypt; abdelaty.mohamed@science.bsu.edu.eg (A.M.R.); husseinnassar300@gmail.com (H.N.H.E.)
* Correspondence: rehabkhaled@science.bsu.edu.eg

Abstract

The persistence of water-soluble polymers such as polyvinylpyrrolidone (PVP) in aquatic environments presents a major challenge for conventional wastewater treatment. Herein, a sunlight-active TiO_2/activated carbon (TiO_2/AC) composite fabricated via a simple physical mixing route is reported for the synergistic adsorption and photocatalytic mineralization of PVP K30. The optimal composite (2:1 weight ratio) exhibits a high surface area (412 m^2 g^{-1}) and an integrated anatase–carbon architecture. The process operates through a sequential "adsorb-and-shuttle" mechanism, whereby PVP is first concentrated on the composite in the dark (30.2% removal in 8 h) and subsequently degraded under solar irradiation. This dual function leads to 86.4% PVP removal and 72.1% total organic carbon (TOC) mineralization, demonstrating true polymer destruction rather than mere surface accumulation. The composite demonstrates robust performance in simulated wastewater, retaining over 68% PVP removal and 55% TOC mineralization in a complex matrix containing competing inorganic ions and natural organic matter. Spectroscopic and thermogravimetric analyses confirm PVP chain scission and near-complete removal of adsorbed residues. An optimized ethanol-washing protocol enables effective catalyst regeneration, with the composite retaining 85% of its initial activity after five cycles. A detailed techno-economic analysis confirms the economic viability of this regeneration strategy at industrial scales (>1000 kg/year), projecting cost savings exceeding 60% compared to fresh catalyst use. Importantly, the PVP-loaded spent TiO_2–AC was successfully repurposed as an electrocatalyst for the urea oxidation reaction, achieving a high current density of 163.7 mA cm^{-2}, which surpasses the performance of the pristine composite. The greenness of the overall process was validated using analytical eco-scale (ESA), method volume intensity (AMVI), and white analytical chemistry (WAC) metrics. Overall, this work presents a sustainable, solar-driven platform that advances a circular economy model, integrating effective polymer wastewater remediation with subsequent energy valorization of the spent material.

Keywords: polyvinylpyrrolidone; titanium dioxide; activated carbon; photocatalysis; mineralization; solar degradation; water treatment; Weste River

Check for updates

Academic Editor: Khursheed B. Ansari

Received: 27 January 2026
Revised: 8 February 2026
Accepted: 13 February 2026
Published: 28 February 2026

Copyright: © 2026 by the authors. Licensee MDPI, Basel, Switzerland. This article is an open access article distributed under the terms and conditions of the Creative Commons Attribution (CC BY) license.

1. Introduction

Owing to its film-forming and stabilizing properties, polyvinylpyrrolidone (PVP K30) is a water-soluble polymer that is extensively used in pharmaceuticals, cosmetics, and food processing [1,2]. However, its widespread application and chemical stability have led to its persistence in aquatic environments, raising concerns similar to microplastic pollution. Conventional wastewater treatments often fail to effectively remove PVP, which can interact with natural organic substances, potentially disrupting aquatic ecosystems [3]. Although PVP is not inherently biodegradable, combining it with biodegradable polymers can improve environmental outcomes, but its environmental persistence remains an issue requiring advanced removal approaches [3,4].

Titanium dioxide (TiO_2)-based heterogeneous photocatalysis is a promising method for degrading persistent organic pollutants such as PVP owing to the oxidative strength and chemical stability of TiO_2 [5,6]. Nonetheless, intrinsic limitations such as rapid recombination of photogenerated carriers and limited pollutant adsorption reduce the effectiveness of TiO_2 over water-soluble polymers. Coupling TiO_2 with activated carbon (AC) enhances degradation via improved adsorption capacity and surface area [7], enabling pollutants to be first adsorbed by AC and then photocatalytically decomposed, thus overcoming these challenges through an "adsorb-and-shuttle" mechanism [8,9].

While TiO_2/AC composites have been extensively studied for dye degradation, research focusing on their application to high-molecular-weight water-soluble polymers (>10,000 Da) such as PVP under natural sunlight and providing robust mineralization evidence (TOC reduction > 70%) beyond mere pollutant reduction remains scarce. Furthermore, practical concerns such as catalyst regeneration for sustainable reuse and end-of-life valorization of spent photocatalysts require more attention [10,11]. Notably, high-molecular-weight polymers like PVP K30 (~40,000 Da) present fundamentally different degradation challenges compared to dyes and small organic molecules (<1000 Da), requiring extensive depolymerization, C–C and C–N bond cleavage, and complete mineralization rather than simple chromophore destruction. The repurposing of spent photocatalyst materials represents an emerging opportunity to address both waste management and resource efficiency challenges.

The residual TiO_2/AC can be used as a catalyst in fuel cells because the organic nature of PVP is a new approach. Fuel cells, particularly urea fuel cells, are considered promising energy conversion technologies because of their simple design, convenience of fuel storage, safe handling, and relatively low working temperatures. Direct urea fuel cells (DUFCs) have garnered considerable interest as promising alternative energy technologies, largely because of the low cost, nontoxicity, and high nitrogen content of urea. These attributes make urea an abundant and effective hydrogen carrier for energy conversion applications [12,13]. As urea is commonly found in various waste streams, such as domestic sewage and agricultural runoff, its electrochemical oxidation offers two benefits: clean energy generation and wastewater remediation [14]. DUFCs present several advantages, including operation under mild conditions, high energy densities, and compatibility with inexpensive, earth-abundant catalysts, all of which support their practical implementation and scalability [15].

Significant research has focused on improving electrocatalysts for the urea oxidation reaction (UOR). Although platinum-based catalysts exhibit high activity, their widespread use is hindered by their high cost and susceptibility to poisoning [11]. Consequently, interest in alternative catalysts based on nonnoble transition metals such as nickel, cobalt, and iron has increased. These materials have shown promising UOR performance, particularly when engineered through doping, alloying, or nanostructuring techniques [16,17]. Urea has recently attracted attention as a fuel since it is safe, economical, readily available, and has

high theoretical energy density, making it a feasible alternative to methanol and hydrogen. Moreover, multifunctional catalytic systems are being developed to achieve simultaneous energy production and degradation of organic pollutants. For example, titanium dioxide supported on activated carbon (TiO_2–AC) has demonstrated the ability to not only catalyze urea oxidation but also breakdown persistent contaminants such as polyvinylpyrrolidone (PVP), thereby offering a dual-function approach for sustainable energy generation and environmental purification. Therefore, the use of TiO_2/AC residue as a low-cost, carbon–metal-oxide catalyst provides a new and sustainable way to increase the electrocatalytic performance of urea fuel cells while minimizing their dependence on noble metals.

Therefore, the use of spent TiO_2/AC/PVP composite residue as a low-cost, carbon–metal-oxide catalyst provides a novel and sustainable circular economy pathway to enhance the electrocatalytic performance of urea fuel cells while minimizing their dependence on noble metals and addressing the challenge of photocatalyst disposal.

This study addresses these critical research gaps through the following integrated approach: This study investigated a physically mixed TiO_2/AC composite (2:1 ratio) for sequential adsorption and solar photocatalytic mineralization of PVP K30. First, we demonstrate complete solar-driven mineralization of high-molecular-weight PVP (40,000 Da) using natural sunlight with rigorous confirmation through total organic carbon (TOC) analysis (72.1% mineralization), thermogravimetric analysis (TGA), and Fourier transform infrared spectroscopy (FTIR) of the catalyst residues—going beyond simple pollutant removal to prove true mineralization. Second, we validate the practical applicability of the system through comprehensive testing in simulated wastewater containing multiple interferents (inorganic ions and humic acid), demonstrating resilience in complex matrices (~70% efficiency retention). Third, we provide detailed techno-economic analysis of an optimized ethanol-based regeneration protocol, quantifying cost savings (up to 63% at industrial scale > 1000 kg/year), material loss (~1.8% per cycle), and demonstrating five-cycle reusability with 85% efficiency retention. Fourth, and most innovatively, we pioneer a waste-to-resource circular economy approach by repurposing the spent TiO_2/AC/PVP composite as an enhanced electrocatalyst for direct urea fuel cells, achieving significantly improved performance (163.7 mA cm^{-2} vs. 103.4 mA cm^{-2} for pristine material) due to favorable interfacial modifications induced by PVP residues. These findings suggest an effective, scalable, and economically viable approach to mitigate the environmental impact of persistent water-soluble polymer pollutants while simultaneously addressing spent catalyst disposal challenges through value-added reuse [11,18]. Finally, the environmental sustainability and analytical greenness of our methodology are rigorously assessed using the analytical eco-scale assessment (ESA), analytical method volume intensity (AMVI), and white analytical chemistry (WAC) approaches, often associated with the RGB-12 algorithm.

2. Results and Discussion

2.1. Catalyst Characterization

2.1.1. BET Surface Area and Porosity Analysis

Nitrogen adsorption–desorption analysis was employed to evaluate the textural properties of TiO_2, activated carbon (AC), and the TiO_2/AC (2:1) composite and the corresponding parameters are summarized in Table 1. As shown in Table 1, the TiO_2/AC composite exhibited a markedly greater BET surface area (412.3 ± 8.9 m^2 g^{-1}) than pure TiO_2 (48.5 ± 2.3 m^2 g^{-1}), reflecting the beneficial influence of synthesized AC incorporation on surface development and pore accessibility. As shown in Figure 1, pure TiO_2 exhibited a mesoporous nature, and a Type II isotherm with an H3 hysteresis loop further confirms the presence of slit-like pores formed by aggregated TiO_2 particles, which limits its adsorption capacity. In contrast, activated carbon had a significantly greater BET surface

area (385.7 m^2/g) and a dominant microporous structure, as indicated by the Type IV isotherm with an H4 hysteresis loop. The TiO_2/AC composite exhibited the highest surface area among the samples (412.3 m^2/g), surpassing that of pure AC [19,20]. The composite demonstrated a type IV isotherm with an H4 hysteresis loop (Figure 1), indicative of a mesoporous structure with slit-like pores, as defined by the IUPAC classification [11]. This enhancement indicates a synergistic interaction between the TiO_2 nanoparticles and the porous carbon matrix. The increased pore volume and intermediate average pore diameter (4.3 nm) suggest that the composite contains both micropores inherited from AC and additional mesopores introduced by the dispersion of TiO_2. This dual micro–mesoporous architecture facilitates the diffusion and accommodation of PVP macromolecules inside the porous network by offering a large number of active sites while reducing mass transfer resistance. By improving the interfacial contact between the pollutant and photoactive sites, which facilitates effective photocatalytic degradation [21,22].

Table 1. BET surface area and porosity parameters of the prepared samples.

Material	BET Surface Area (m^2/g)	Total Pore Volume (cm^3/g)	Average Pore Diameter (nm)
TiO_2	48.5 ± 2.3	0.062 ± 0.004	5.1 ± 0.3
Activated Carbon	385.7 ± 7.2	0.402 ± 0.011	3.9 ± 0.2
TiO_2/AC	412.3 ± 8.9	0.438 ± 0.013	4.3 ± 0.2

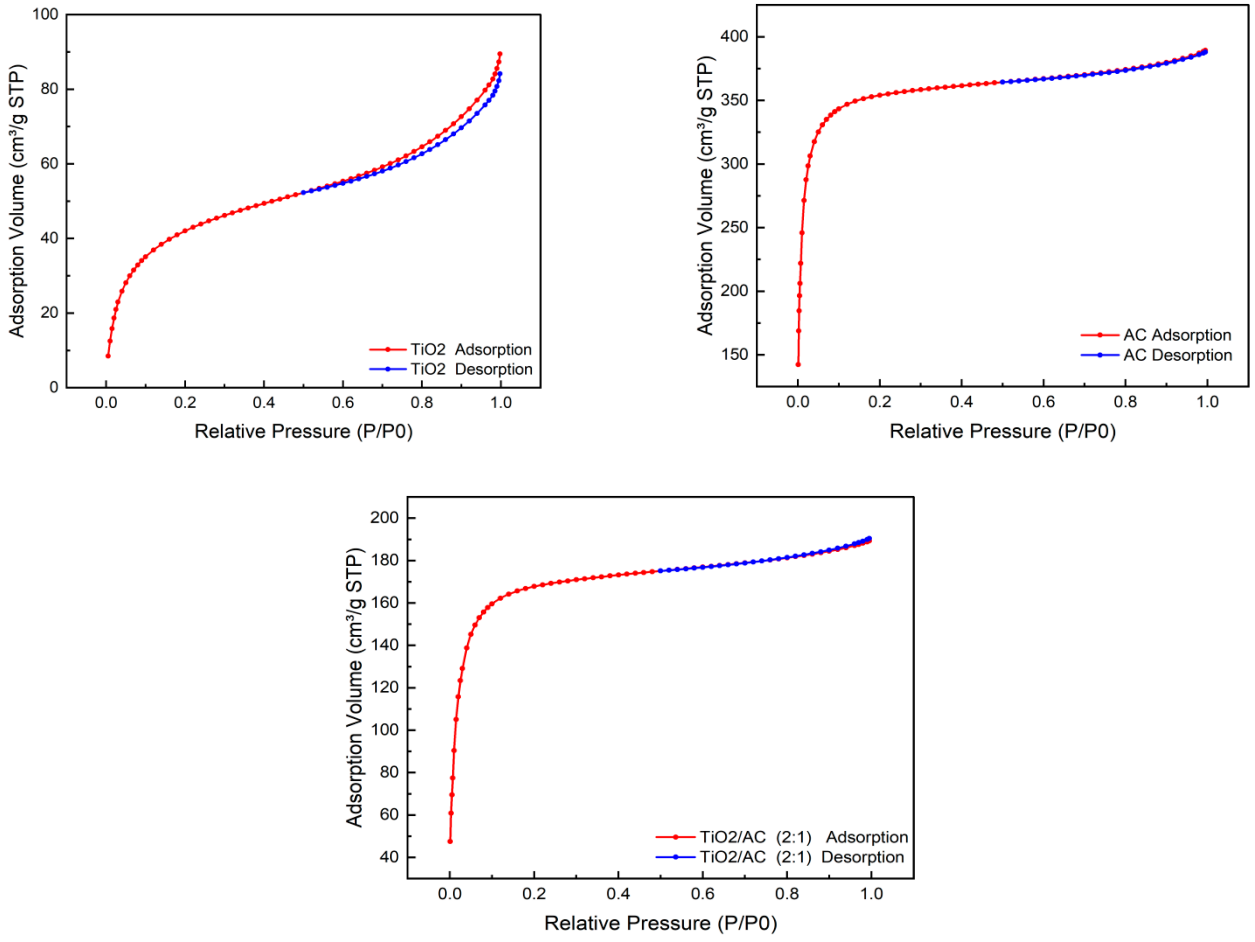

Figure 1. Nitrogen adsorption–desorption isotherms of TiO_2, activated carbon (AC), and TiO_2/AC.

2.1.2. XRD Analysis

The X-ray diffraction (XRD) patterns distinctly reveal the structural signatures of each component and elucidate how interfacial assembly influences crystallographic features. As shown in Figure 2, activated carbon (AC) has two distinct diffraction peaks at 2θ = 24.41° and 2θ = 43.11°, which correspond to the (002) and (100) crystal planes [23]. In addition, TiO_2 displays the anatase phase, with distinct diffraction peaks at 2θ= 25.3°, 37.8°, 48.0°, 53.9°, 55.0°, and 62.7°, which correspond to the 101, 004, 200, 105, 211, and 204 crystal planes, respectively [24]. In the TiO_2–AC composite, the (101) and (200) reflections slightly shift to lower 2θ values and noticeably broaden. These changes correspond to d-spacing for the (101) and (200) planes. There is a noticeable decrease in peak intensity for TiO_2–AC, and this decrease suggests a reduction in crystallinity due to the incorporation of amorphous activated carbon. Following PVP adsorption (TiO_2–AC/PVP), both reflections undergo an additional leftward shift and further broadening, culminating in total lattice expansions of 101,200 relative to pristine TiO_2. This evolution is consistent with polymer capping and coordination [25].

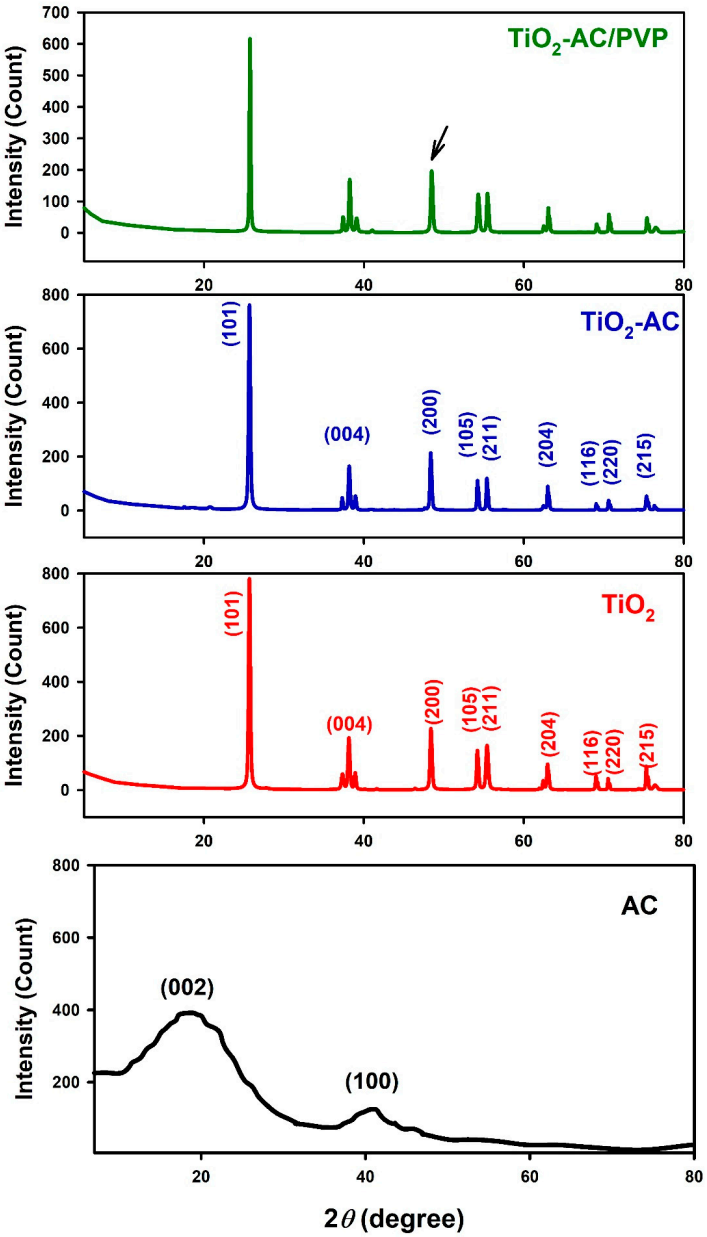

Figure 2. XRD patterns of the TiO_2, AC, TiO_2–AC, and TiO_2–AC/PVP composites.

The crystallite size of the synthesized TiO_2–AC composite was estimated to be 37.66 nm, whereas that of TiO_2–AC–PVP was 26.76 nm, as calculated from the XRD data via the Debye–Scherrer equation. The decrease in crystallite size suggested agglomeration after PVP incorporation. Additionally, the interaction between PVP functional groups and TiO_2–AC surfaces can facilitate particle coalescence. The interplanar spacing (d-spacing) values calculated from the XRD analysis revealed that the TiO_2–AC composite presented a d-spacing of 0.3455 nm, whereas the TiO_2–AC/PVP sample presented a slightly greater value of 0.3462 nm. The slight increase in d-spacing after the incorporation of polyvinylpyrrolidone (PVP) indicates a slight expansion in the TiO_2 lattice planes.

2.1.3. FTIR Analysis

The FT-IR spectra provide molecular-level insight into the evolution of surface and interfacial chemistry during the adsorption process. Figure 3 shows the FT-IR spectra of the samples. The FT-IR spectrum of activated carbon (AC) displays prominent peaks at 3420 cm^{-1} and 3140 cm^{-1}, which are assigned to the stretching vibrations of hydroxyl (–OH) groups. The peak at 1630 cm^{-1} is associated with the stretching vibration of the –OH group, whereas the band at 1400 cm^{-1} is attributed to C=O stretching. A minor band at 611 cm^{-1} is related to C–C skeletal vibrations [14,15]. In the FT-IR spectrum of TiO_2, the broad absorption bands observed between 3405 cm^{-1} and 3151 cm^{-1} are indicative of surface hydroxyl groups (–OH) and adsorbed water molecules. The absorption band at 1629 cm^{-1} corresponds to the bending vibration of molecular water, whereas the band near 1400 cm^{-1} is characteristic of coordinatively bound water. Additionally, a broad band centered at 541 cm^{-1} is attributed to Ti–O stretching vibrations [12,13].

In the FT-IR spectrum of the TiO_2–AC composite, the O–H stretching region is retained but appears less intense than that of the individual components. The lattice vibration region exhibited Ti–O and Ti–O–Ti stretching modes, with maxima at approximately 661 cm^{-1} and 510 cm^{-1}, confirming the successful incorporation of TiO_2 into the carbon matrix [26]. Compared with pristine AC, subtle modifications in the 1200–1000 cm^{-1} region, such as the appearance of shoulders or increased intensity, suggest the formation of interfacial Ti–O–C bonds, which are commonly reported in TiO_2/AC hybrid materials and indicate strong interfacial coupling between the two phases [11,16]. Following the adsorption of polyvinylpyrrolidone (PVP), a distinct amide I (C=O) band emerges near 1660 cm^{-1}, accompanied by PVP-related C–N/amide absorptions in the 1285–1295 cm^{-1} range and CH_2 deformation bands at approximately 1460 cm^{-1}. The broad O–H stretching envelope between 3500 cm^{-1} and 3100 cm^{-1} typically becomes narrower and less intense, reflecting hydrogen bonding interactions. Small downshifts and changes in the intensity of the amide I band are characteristic of hydrogen bonding between PVP and oxide Lewis acid sites (such as Ti^{4+}) or surface –OH groups, confirming the adsorptive interaction of PVP with the TiO_2–AC composite [17,27].

2.1.4. SEM Analysis

The TiO_2 nanostructure (Figure 4a) micrograph reveals dominant intergroup nanorods, which assemble into a porous structure. The crystallites exhibit sharp faceting, relatively uniform diameters, and high aspect ratios. Anisotropic crystal growth drives the formation of needle- and rod-like aggregates with hierarchical porosity [28]. The surface of the activated carbon (Figure 4b) has a porous structure [29]. Activated carbon has aggregated irregular surfaces with many micropores and crevices of various sizes at the surface [30]. In the TiO_2–AC composite (Figure 4c), many TiO_2 nanorods grow in a conformal manner along the carbon matrix [31]. In the TiO_2–AC composite structure, TiO_2 agglomerates are highly dispersed in the AC matrix. TiO_2–AC after PVP loading (Figure 4d), the surface

appears smoother and partially coated: carbon wrinkles are enveloped, and interparticles are blunted. This transformation is consistent with the formation of a thin polymer layer that spreads over both the carbon substrate and the oxide features, resulting in a more continuous film that bridges nanoscale gaps and rounds sharp asperities [32].

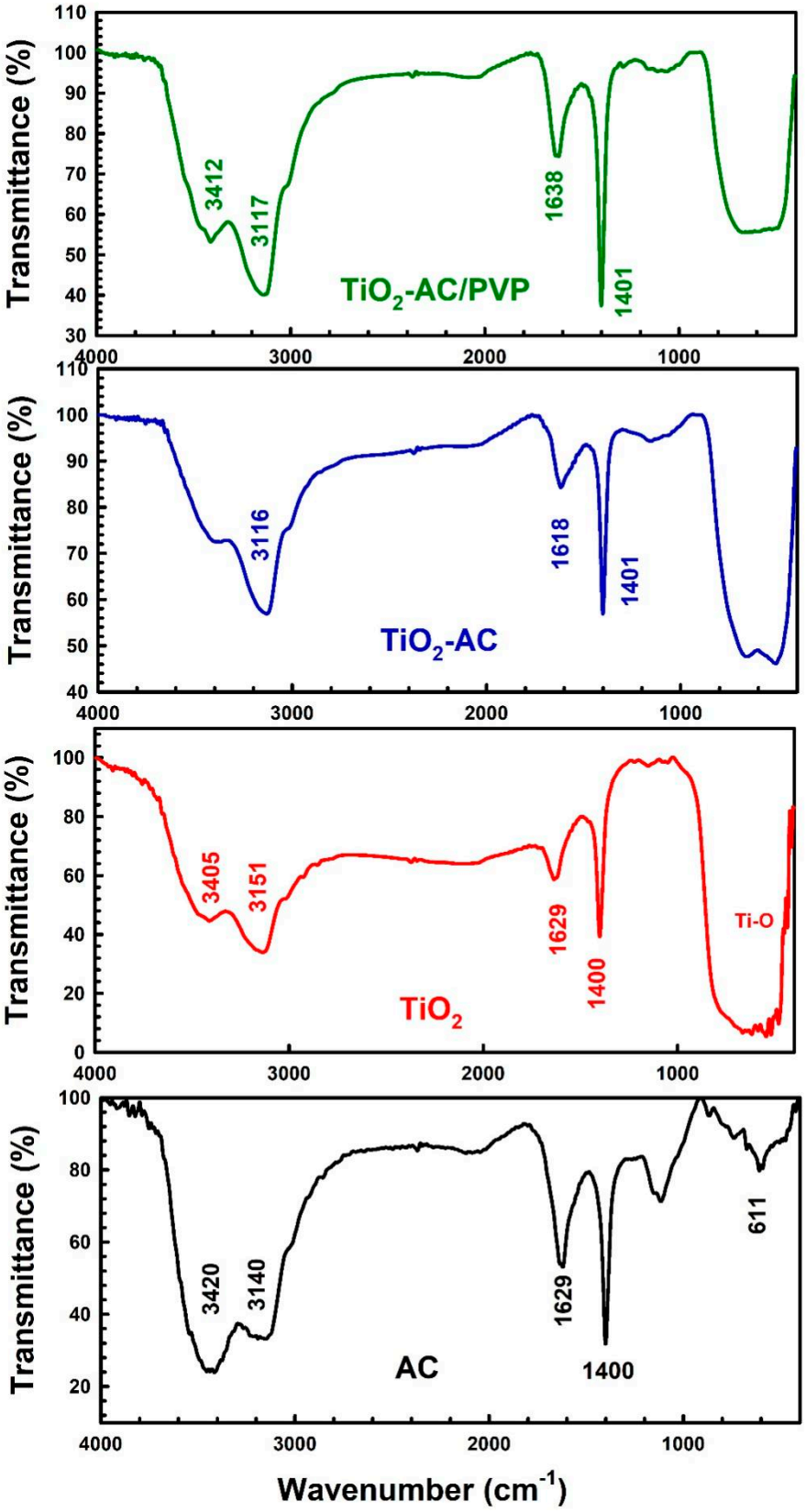

Figure 3. FTIR spectra of TiO_2, AC, TiO_2–AC, and TiO_2–AC/PVP composites.

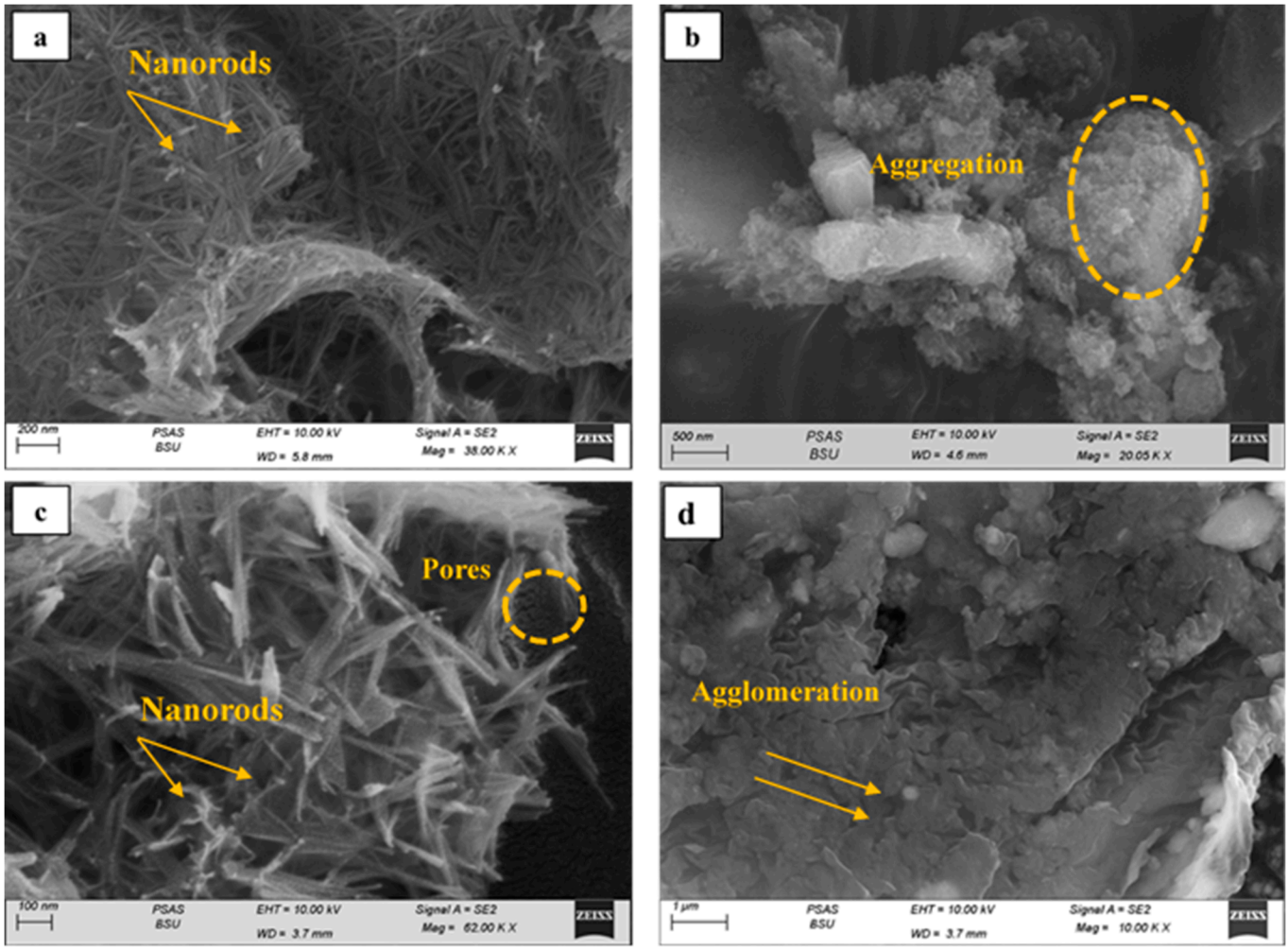

Figure 4. SEM images of the (**a**) TiO_2, (**b**) AC, (**c**) TiO_2–AC, and (**d**) TiO_2–AC/PVP composites.

2.1.5. TGA

Thermogravimetric analysis (TGA) was performed via a TGA Q50 (TA Instruments, New Castle, DE, USA) under an air atmosphere (flow rate: 60 mL/min) at a heating rate of 10 °C/min from 30 to 800 °C, employing a sample mass of approximately 5–10 mg. The obtained TGA profiles and mass loss data for the principal samples are illustrated in Figure 5. The TGA curves revealed distinct thermal behaviors for the pure components and composite materials. Pure TiO_2 exhibited minimal weight loss (~5%) throughout the heating range, confirming its high thermal stability [33]. In contrast, activated carbon (AC) showed a pronounced weight loss of approximately 80.1% between 350–500 °C, which corresponds to the combustion of carbonaceous material, resulting in approximately 9.0% residual ash content. For the TiO_2–AC (2:1) composite, the total mass loss was significantly lower (25.0% up to 600 °C), reflecting the incorporation of thermally stable TiO_2 [34]. The major decomposition occurred between 300–600 °C, where a 16.5% loss was recorded, which was attributable to the oxidation of the carbonaceous fraction of the composite. Upon PVP adsorption (TiO_2–AC/PVP), the mass loss in the 400–600 °C zone increased sharply to 41.2%, indicating substantial incorporation of the organic polymer within the porous matrix. The additional 24.7% mass loss (relative to that of the fresh composite) corresponds to the degradation of adsorbed PVP and associated moisture, quantitatively confirming successful polymer adsorption. After 48 h of sunlight exposure, the mass loss in the combustion zone decreased markedly to 18.0%, closely approaching that of the pristine composite (16.5%). This minimal difference (~1.5%) reflects the effective photodegradation

and mineralization of adsorbed organics during photocatalytic treatment, demonstrating the catalyst's efficient regeneration capability and structural resilience.

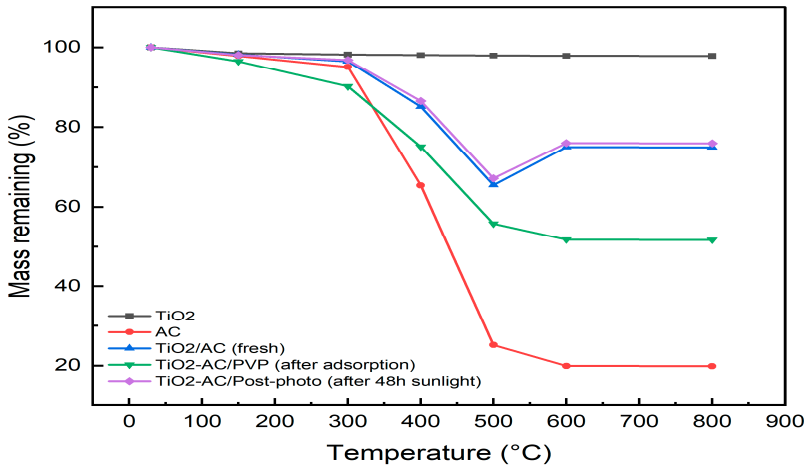

Figure 5. TGA curves of TiO_2, AC, the TiO_2/AC composite, the PVP-loaded composite, and the composite after 48 h of sunlight exposure.

2.2. Adsorption Performance

The adsorption behavior of polyvinylpyrrolidone (PVP K30) onto the TiO_2/Activated Carbon (TiO_2/AC) composite was systematically investigated by evaluating the effects of critical parameters, including the solution pH, adsorbent dosage, and initial pollutant concentration. The equilibrium and kinetic data were analyzed via established models to elucidate the underlying mechanisms.

2.2.1. Effects of pH and Adsorbent Dosage

The pH of the solution is a critical parameter governing adsorption efficiency, as it influences the surface charge of the adsorbent and the ionization state of the PVP macromolecules. As illustrated in Figure 6a, the maximum PVP removal efficiency of 30.2% was achieved at a natural pH of 6.0. This optimal performance can be attributed to favorable coordinative bonding between the carbonyl oxygen of PVP and the Lewis acid sites (Ti^{4+}) on the TiO_2 surface, alongside reduced electrostatic repulsion [35]. At a lower pH (2.0), the protonated, positively charged adsorbent surface repels the partially positive pyrrolidone ring, reducing adsorption. Under highly alkaline conditions (pH 10), the PVP chain may adopt a coiled conformation, limiting the accessibility of its functional groups.

The effect of adsorbent dosage was studied, and the results, illustrated in Figure 6b, revealed that the PVP removal efficiency increased with increasing adsorbent mass, from 11.5% at 0.05 g to 30.2% at 0.20 g, due to the greater availability of adsorption sites. Conversely, the adsorption capacity decreased from 23.00 to 11.30 mg/g over the same range, a common phenomenon attributed to particle aggregation and site saturation at higher doses [36]. A dosage of 0.20 g was selected as the optimal compromise for all subsequent experiments, yielding a removal efficiency of 30.2% with a capacity of 15.10 mg/g.

2.2.2. Adsorption Isotherms and Kinetics

A thorough analysis of the adsorption kinetics and equilibrium isotherms is crucial for understanding the mechanism, efficiency, and practical potential of the adsorption process, revealing the rate-controlling steps and the nature of the interactions between PVP K30 and the TiO_2/AC composite.

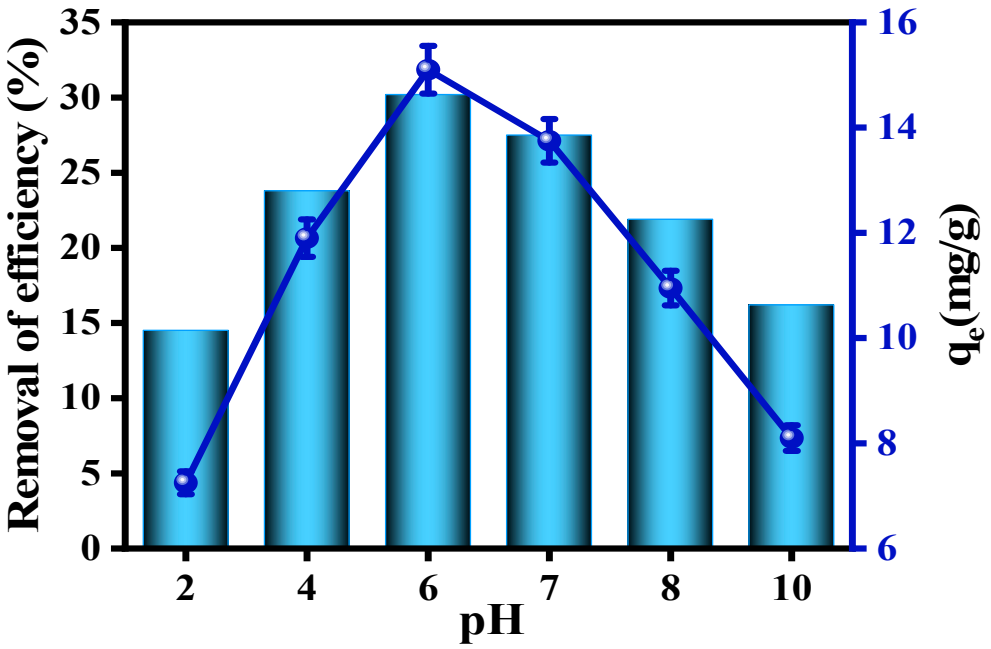

(**a**)

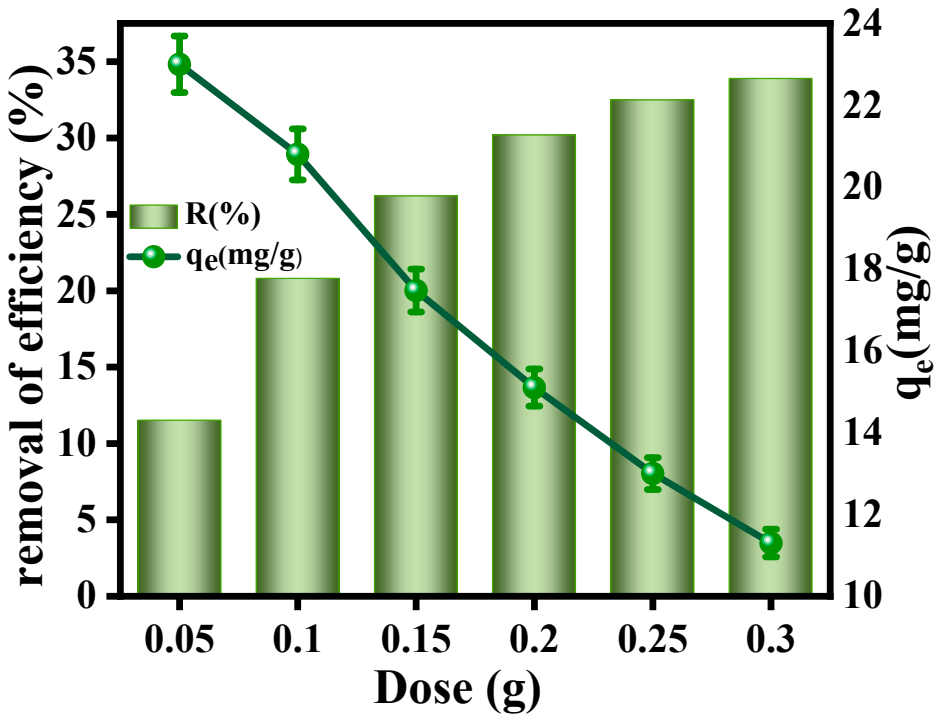

(**b**)

Figure 6. Influence of (**a**) pH and (**b**) adsorbent dosage on PVP removal.

Adsorption Isotherms

Adsorption isotherms describe the distribution of pollutant molecules between the solid and liquid phases at equilibrium. To identify the dominant adsorption mechanism, the experimental data were fitted to three fundamental models: Langmuir (monolayer adsorption on homogeneous sites), Freundlich (multilayer adsorption on heterogeneous surfaces), and Sips (a hybrid model that transitions between Langmuir and Freundlich behavior).

As summarized in Table 2, the Sips (Langmuir–Freundlich) isotherm provided the best fit (R^2 = 0.992), indicating a hybrid adsorption mechanism. The model reveals that at low concentrations, adsorption resembles Freundlich-type behavior, suggesting initial multilayer uptake on the heterogeneous carbon surface. At higher concentrations, it approaches Langmuir-type saturation, implying the filling of specific, homogeneous active sites. The maximum adsorption capacity (q_{max}) predicted by the Sips model was 45.8 mg g^{-1}, and the heterogeneity factor (n_s = 0.95) close to 1 indicates that the composite surface behaves nearly as a homogeneous Langmuir system. This supports the conclusion that the primary chemisorption sites—likely the well-dispersed TiO_2 nanoparticles—are relatively uniform [37].

Table 2. Isotherm model parameters for the adsorption of PVP onto the TiO_2/AC composite.

Isotherm Models	Expression	Parameters	TiO_2/AC
Langmuir	$q_e = q_{max}\frac{KLC_e}{1+KLC_e}$	q_{max} (mg/g)	48.50
		K_L	0.045
		R^2	0.978
Freundlich	$q_e = K_f C_e^{1/n}$	K_f	4.12
		$1/n_f$	0.541
		R^2	0.963
Sips	$qe = \frac{q_{max}K_sC_e^{ns}}{1+K_sC_e^{ns}}$	q_{max} (mg/g)	45.8
		K_S	0.051
		n_s	0.95
		R^2	0.992

The Langmuir model also provided a good fit (R^2 = 0.978), supporting the concept of monolayer adsorption at higher coverage. The Freundlich model yielded a lower correlation (R^2 = 0.963), confirming that purely heterogeneous multilayer adsorption is not the dominant mechanism. Detailed parameters for additional isotherm models (Temkin, Redlich-Peterson, Baudu, Fritz-Schlunder, Dubinin-Radushkevich, and Jossens) are provided in Table S1 of the Supplementary Information. The high adsorption capacity underscores the vital role of the AC matrix in concentrating PVP macromolecules within its porous structure, thereby preconditioning the pollutant for subsequent photocatalytic degradation (Figure 7). A comprehensive statistical analysis of all fitted isotherm models, including SSE, RMSE, MAE, and hybrid error functions, is provided in Table S2 of the Supplementary Information.

Adsorption Kinetics

The adsorption profile of PVP onto the TiO_2/AC composite exhibited characteristic two-phase behavior: an initial rapid uptake within the first 120 min, followed by a gradual approach to equilibrium within 480 min (8 h) (Figure 8). The rapid initial phase is attributed to the abundance of vacant active sites on the adsorbent surface, while the subsequent slower phase is controlled by the diffusion of PVP macromolecules into the mesoporous structure of the composite.

To elucidate the adsorption mechanism, the kinetic data were fitted to pseudo-first-order (PFO), pseudo-second-order (PSO), and intraparticle diffusion (IPD) models, Table 3. The PSO model provided the best fit (R^2 = 0.998), with a calculated equilibrium capacity (q_e, cal = 15.87 mg g^{-1}) closely matching the experimental value (q_e, exp = 15.10 mg g^{-1}). This strongly indicates that chemisorption (involving coordinative bonding between the

PVP carbonyl groups and TiO_2 Lewis acid sites, as suggested by FTIR analysis) was the rate-limiting step.

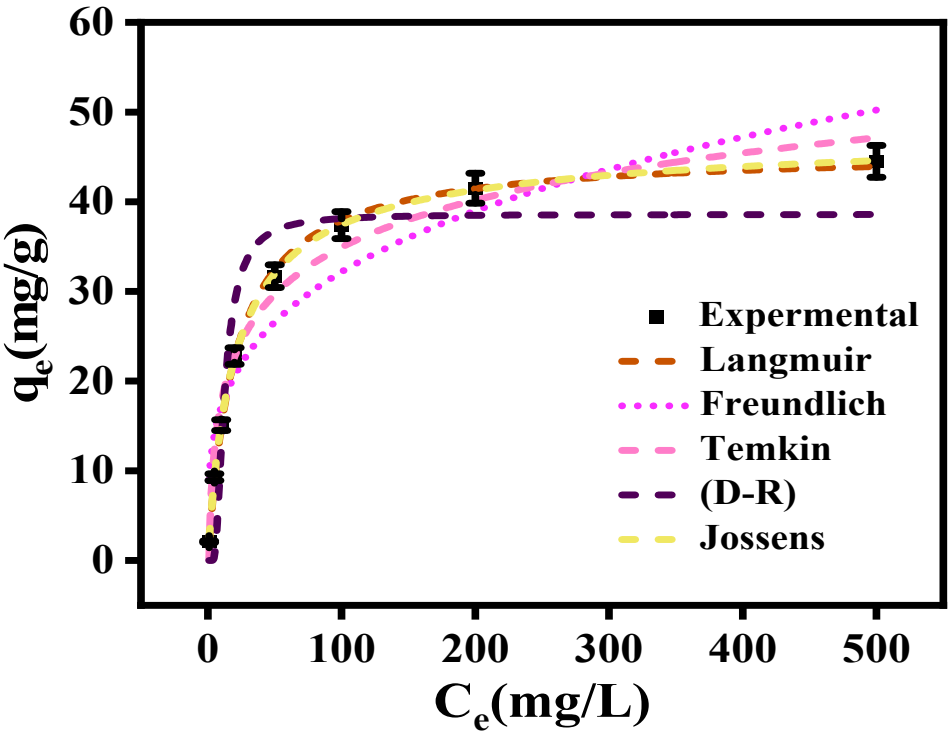

Figure 7. Adsorption isotherms of PVP onto TiO_2/AC.

Table 3. Parameters of the kinetic models for the adsorption of PVP onto the TiO_2/AC composite.

Kinetic Models	Equation	Parameters	TiO_2/AC
Pseudo first Order	$q_t = q_e(1 - e^{-K_1 t})$	k_1	0.0087
		$q_{e\ (mg/g)}$	15.25
		R^2	0.945
Pseudo second Order	$q_t = \frac{q_e^2 K_2\ t}{1+\ q_e\ K_2 t}$	k_2	0.0012
		$q_{e\ (mg/g)}$	15.87
		R^2	0.998

IPD								
Step 1			**Step2**			**Step3**		
k_P1	C_1	R^2	k_P1	C_1	R^2	k_P1	C_1	R^2
1.23	0.571	0.975	0.191	11.67	0.849	0.0007	15.079	0.294

The intraparticle diffusion model (IPD) revealed a multi-stage process with a significant intercept (C = 6.81), confirming that intraparticle diffusion was not the sole controlling step and that film diffusion also contributed to the overall kinetics [38]. Parameters for additional kinetic models (Elovich, Avrami, and Mixed 1,2-order) are provided in Table S3 of the Supplementary Information.

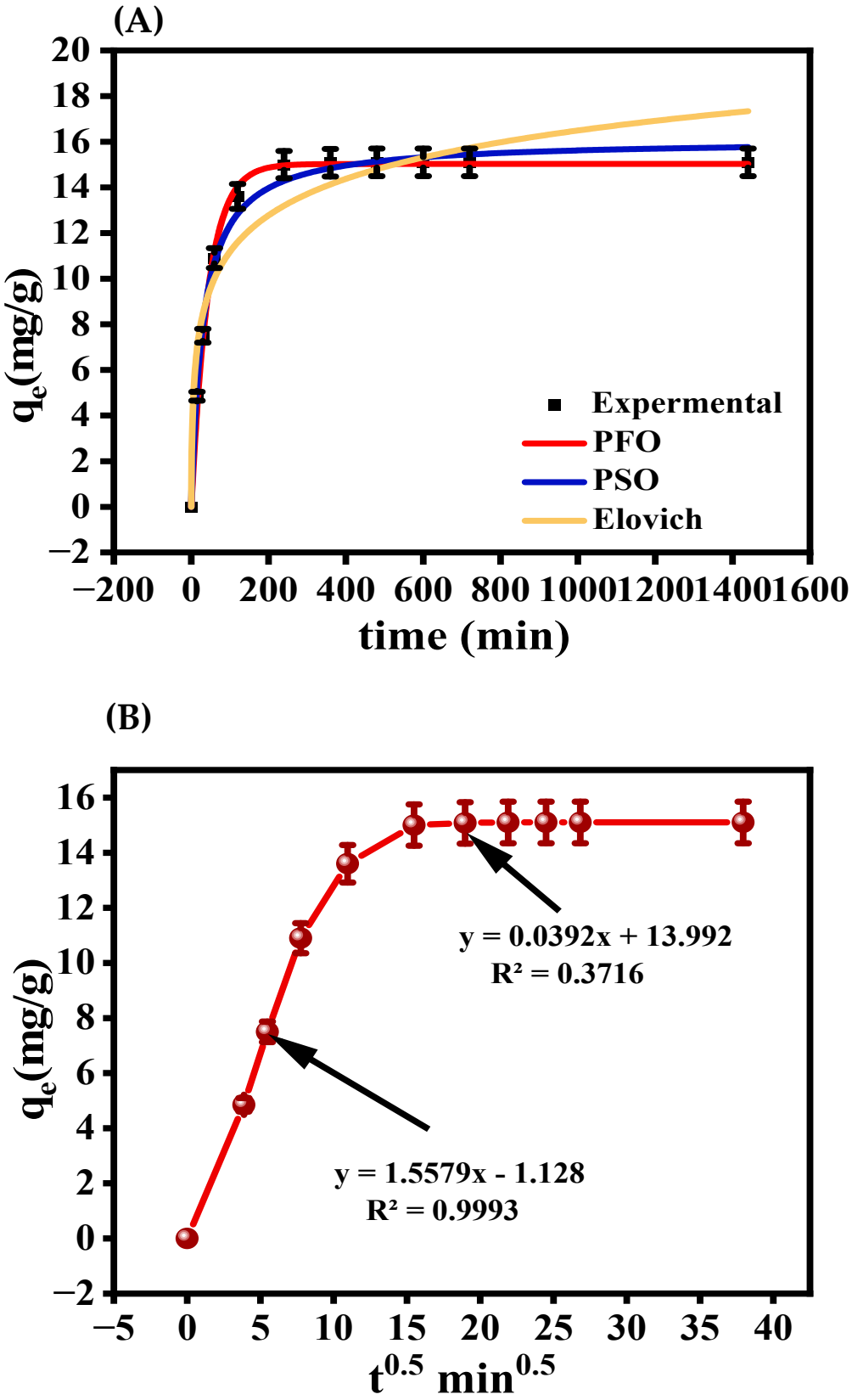

Figure 8. Adsorption kinetics of PVP on TiO_2/AC (**A**) pseudo-first-order (PFO), pseudo-second-order (PSO) and Elovich and (**B**) for the intra partical diffusion (IPD).

2.3. Anti-Interference Performance in Simulated Wastewater

The practical deployment of photocatalytic materials necessitates robust performance in complex aqueous matrices beyond idealized laboratory conditions. To evaluate this, the

TiO_2/AC composite was tested in three simulated wastewater systems containing common interferents: an inorganic ion matrix (IIM), a natural organic matter matrix (NOMM), and a mixed matrix (MM) combining both.

2.3.1. Effect of Inorganic Ions

After 8 h of sunlight irradiation, PVP removal efficiency decreased from 86.4% in deionized water to 78.5% in the IIM (Figure S1a), while TOC mineralization decreased from 72.1% to 65.3%, as illustrated in Figure S1b. The apparent rate constant (k_{app}) decreased by approximately 19%, Figure S1c. This inhibition is attributed to: (1) competition for active sites (especially by HCO_3^-), (2) radical scavenging (HCO_3^-/CO_3^{2-} reacting with •OH to form less reactive $CO_3\bullet^-$), and (3) increased ionic strength affecting electrostatic interactions. Despite this, the composite retained ~91% of its original efficiency, demonstrating good ionic interference resistance, primarily due to the AC component's ability to concentrate PVP near TiO_2 sites via the "adsorb-and-shuttle" mechanism.

2.3.2. Effect of Natural Organic Matter

The presence of humic acid (HA) as a model NOM caused a more pronounced inhibition compared to inorganic ions. In the NOMM, the PVP removal efficiency decreased to 71.2% (Figure S2a) and the TOC mineralization was reduced to 59.4% (Figure S2b) after 8 h of solar irradiation, representing an approximate 33% reduction in the apparent rate constant compared to deionized water. This stronger inhibitory effect stems from: (1) competitive adsorption of high-molecular-weight HA onto the AC and TiO_2 surfaces, blocking active sites; (2) light screening (the "inner filter" effect) by the colored HA, reducing photon flux to the catalyst; (3) scavenging of photogenerated radicals by the phenolic and quinone moieties present in HA; and (4) potential surface fouling by large organic aggregates. Notably, the measured TOC reduction includes the partial mineralization of HA itself, indicating the composite retains non-selective oxidative capability even in complex organic matrices.

2.3.3. Performance in Mixed Matrix Simulated Wastewater

In the most challenging MM environment, PVP removal efficiency was 68.9% with 55.1% TOC mineralization, representing a ~38% reduction in degradation rate. The interference effects were partially additive. Crucially, as summarized in Figure S3a,b, the composite retained ~80% of its original PVP removal capacity and ~76% of its TOC mineralization ability. The degradation kinetics remained first-order, and the AC matrix provided a buffering effect by maintaining high local PVP concentrations. This performance underscores the material's potential utility as a polishing step in multi-barrier treatment trains for complex wastewaters.

2.4. Photocatalytic Degradation and Mineralization Under Sunlight

The efficacy of the TiO_2/AC composite was evaluated through a sequential adsorption–photocatalysis process for the solar-driven remediation of PVP, and the results are detailed in Figure 9. The process began with an 8-h dark adsorption phase, resulting in a 30.2% reduction in the PVP concentration. Upon exposure to natural sunlight, a pronounced acceleration in pollutant removal was observed, culminating in a total PVP elimination of 86.4% after 48 h. This dramatic increase under irradiation confirms the catalytic function of the composite beyond mere adsorption.

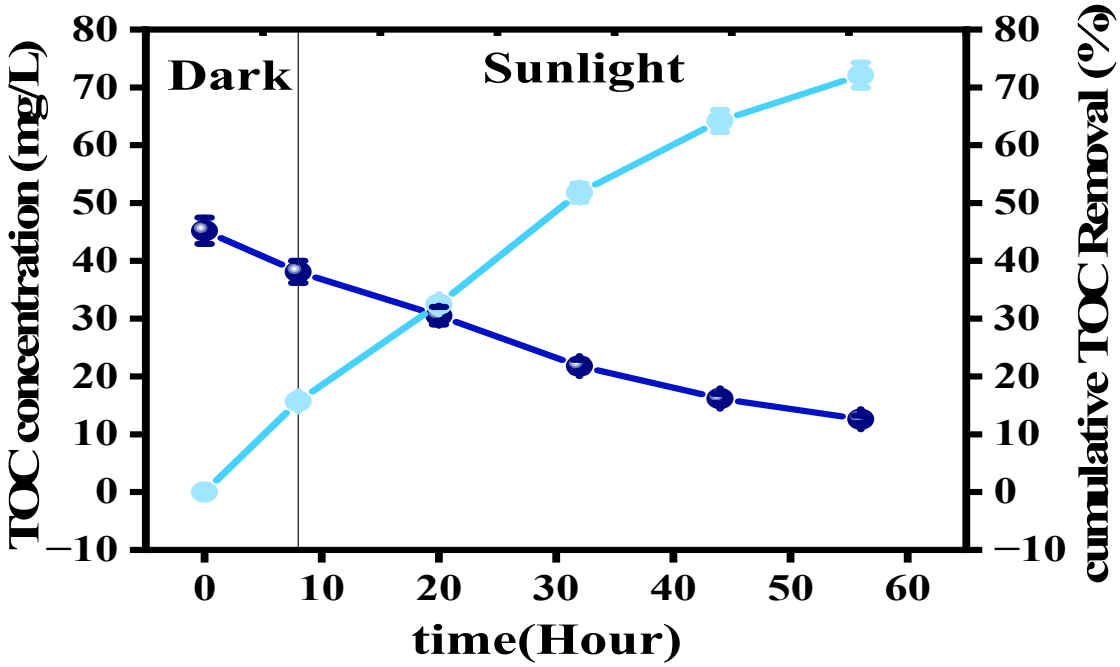

Figure 9. Time-dependent reduction in the TOC concentration and cumulative mineralization of PVP during the sequential adsorption–photocatalysis process.

Control experiments are critical for confirming the synergistic mechanism involved. Negligible degradation (<5%) was observed for PVP solutions under sunlight without a catalyst, confirming the inherent resistance of the polymer to direct photolysis [18]. When activated carbon alone was used in the dark, removal plateaued at approximately 35%, which was attributable solely to adsorption, confirming its nonphotocatalytic nature. Pure TiO_2 under sunlight has a limited removal efficiency of 42%, which is constrained by its poor adsorption capacity and rapid recombination of photogenerated charge carriers [39,40]. The TiO_2/AC composite kept in darkness reached a plateau of ~30% removal, identical to the initial adsorption phase, confirming that significant degradation is a light-dependent process.

The superior performance is attributed to a well-established "adsorb and shuttle" mechanism. The activated carbon component acts as a high-capacity adsorbent, concentrating PVP macromolecules close to the photocatalytic sites on the TiO_2 nanoparticles [41]. Under solar irradiation, TiO_2 generates electron–hole (e^-/h^+) pairs. The conductive carbon matrix functions as an efficient electron sink, accepting photogenerated electrons and thereby significantly suppressing charge carrier recombination [42]. This crucial separation prolongs the lifetime of highly oxidizing valence band holes (h^+), which can directly oxidize PVP or, more importantly, react with surface hydroxyls or water to generate hydroxyl radicals (•OH) [39,43]. These nonselective •OH radicals are the primary species responsible for the systematic oxidative scission of the PVP polymer chain [44].

The most compelling evidence for complete pollutant breakdown was provided by total organic carbon (TOC) analysis. While HPLC tracked the disappearance of the parent PVP compound, TOC quantification verified the destruction of the organic carbon skeleton. The TOC content decreased from 45.2 mg/L to 12.6 mg/L over 48 h, corresponding to a mineralization degree of 72.1%. This high level of mineralization, which converts organic carbon to CO_2 and water, is a critical metric for advanced oxidation processes, as it confirms the elimination of potentially persistent and toxic organic intermediates from the aqueous system [39,43]. The progressive TOC removal demonstrated the composite's effectiveness for deep oxidation under natural sunlight.

2.5. Proposed Degradation Mechanism and Pathway

Based on the experimental evidence obtained in this study, a plausible degradation pathway for PVP under solar irradiation is proposed. The process begins with the experimentally demonstrated adsorption and concentration of PVP macromolecules on the composite surface, primarily through carbonyl coordination to Ti^{4+} Lewis acid sites (as indicated by FTIR shifts) and hydrophobic interactions with the carbon matrix [11,18].

Under solar irradiation, the photocatalytic activity of TiO_2, coupled with the electron-accepting capacity of activated carbon, leads to the generation of charge carriers. While radical scavenging experiments were not conducted in this study, the significant TOC mineralization (72.1%) observed strongly suggests the involvement of highly oxidizing species. Based on well-established photocatalytic mechanisms of TiO_2 systems and the complete mineralization achieved, it is plausible that hydroxyl radicals (•OH) and/or superoxide radicals ($\bullet O_2^-$) are generated and participate in the degradation process [39,43,45–48].

The proposed pathway involves initial oxidative scission at the tertiary carbon atoms adjacent to nitrogen in the pyrrolidone ring, leading to polymer chain fragmentation [18,44]. This is followed by ring opening and eventual mineralization to CO_2, H_2O, and nitrate/nitrite ions, as evidenced by the substantial TOC reduction [48].

The minimal residual organic content observed in post-reaction TGA/FTIR analyses supports the near-complete degradation of adsorbed PVP [18].

It should be noted that while this pathway is consistent with our experimental data and general photocatalytic principles, definitive identification of reactive species and intermediate compounds would require additional characterization techniques such as electron paramagnetic resonance (EPR) spectroscopy for radical detection or liquid chromatography–mass spectrometry (LC–MS) for intermediate analysis. Future studies employing these techniques could further validate the proposed mechanism.

In summary, the high degree of mineralization confirmed by TOC analysis provides strong evidence for complete PVP degradation, while the specific mechanistic details presented here represent a reasonable hypothesis consistent with both our experimental observations and established photocatalytic literature [39,43,45–48].

2.6. Catalyst Regeneration Optimization, Economic Analysis, and Reusability

The practical deployment and environmental sustainability of the TiO_2/AC composite necessitate an efficient and cost-effective regeneration strategy. This section details the systematic optimization of an ethanol-washing protocol and presents a techno-economic assessment to evaluate its scalability and practical reuse potential.

2.6.1. Optimization of Regeneration Parameters

The influence of key operational parameters on catalyst activity retention was systematically investigated (Table S4a–d). The results identified optimal regeneration conditions as: 95% ethanol, a washing duration of 30 min, an ethanol-to-catalyst ratio of 30:1 (mL/g), and a drying temperature of 80 °C. Under these conditions, the composite retained 94.2% of its initial photocatalytic activity and restored the BET surface area to 410 m^2/g. Drying at temperatures $\geq$ 120 °C induced a marked decline in both activity and surface area, indicating structural degradation. Consequently, the established regeneration protocol is: wash the spent catalyst with 95% ethanol (30:1 v/w) for 30 min, filter, and dry at 80 °C for 4 h.

2.6.2. Ethanol Recovery, Physical Loss, and Energy Consumption

To ensure economic and operational sustainability, a closed-loop distillation system was implemented for ethanol recovery. The gravimetrically determined recovery rate

averaged 92.7 ± 0.9% over five consecutive cycles. Physical catalyst loss, measured by mass difference after each regeneration cycle, averaged 1.84 ± 0.15% per cycle, resulting in a cumulative loss of 9.22% after five cycles (Table S5). Energy consumption was estimated from laboratory-scale operations; scaling projections indicate that industrial implementation with heat integration could reduce specific energy consumption by over 90%.

2.6.3. Techno-Economic and Environmental Impact Analysis

A scaled cost–benefit analysis was performed to assess economic viability (Table S6). The analysis shows that regeneration becomes economically favorable over fresh catalyst synthesis at annual throughputs exceeding 1000 kg. At an industrial scale of 10,000 kg/year, the estimated regeneration cost is $4.60/kg, compared to $12.30/kg for fresh catalyst, yielding a 63% cost saving. For a representative 10,000 L/day wastewater treatment plant, this translates to annual savings of ~$21,870, with an estimated return on investment (ROI) payback period of ~8 years. Beyond economic gains, the regeneration strategy significantly reduces raw material consumption and solid waste, lowering the overall environmental footprint.

2.6.4. Reusability Performance

Employing the optimized regeneration protocol, the TiO_2/AC composite was subjected to five consecutive adsorption–photocatalysis–regeneration cycles. As shown in Figure 10, the composite maintained a high PVP removal efficiency of 84.1% in the fifth cycle, representing 85% activity retention relative to the first cycle (86.4% removal). This marginal decline aligns closely with the quantified physical catalyst loss (~9.22% cumulative mass loss), confirming the robustness and practical effectiveness of the regeneration strategy.

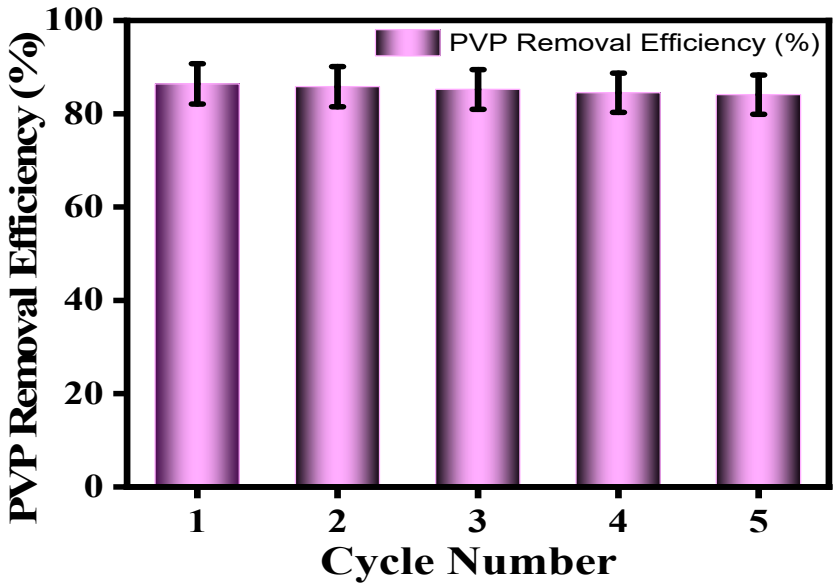

Figure 10. PVP removal efficiency across multiple regeneration cycles.

2.7. Recycling Waste TiO_2–AC as a Catalyst

To investigate the reuse of the spent adsorbent, the performance of the TiO_2–AC/PVP samples was tested as electrocatalysts under different reaction conditions.

2.7.1. Electrochemical Activity in 1 M KOH

Effects of Different Urea Concentrations on Electrochemical Oxidation

The influence of the urea concentration on the electrocatalytic response of the TiO_2–AC electrode was systematically evaluated via cyclic voltammetry. As depicted in Figure 11A,

the anodic current density progressively increased with increasing urea concentration, reaching a peak value of 103.44 mA/cm^2 at the highest tested concentration of 1.0 M urea for TiO_2–AC. This increase indicates that elevated urea concentrations increase the availability of reactant molecules at the electrode/electrolyte interface, thereby accelerating the kinetics of the urea oxidation reaction [49–53]. The integration of TiO_2 with a conductive activated carbon support is well established to increase the density of accessible electroactive sites and facilitate electron transport through the porous carbon matrix, effectively reducing polarization losses and enhancing current generation during urea oxidation [54,55]. As illustrated in Figure 11B, the TiO_2–AC/PVP electrode exhibited a pronounced increase in current density with increasing urea concentration, attaining a peak value of 163.7 mA/cm^2 at 1.0 M. This represents a significant enhancement relative to the preadsorption of approximately 103.7 mA/cm^2 for TiO_2–AC. These findings demonstrate that the PVP layer does not impede charge transfer, thereby improving wettability, facilitating electrolyte infiltration, and sustaining continuous ionic conduction at the electrode/electrolyte interface [56–59]. This improved interfacial wetting promotes accelerated urea transport to catalytically active sites and stabilizes a larger population of electroactive regions on the catalyst surface. PVP also aids in the stabilization of reaction intermediates and the favorable adsorption and motion of urea molecules at the catalyst surface, both of which enhance catalytic kinetics and increase electrochemical activity. Particular interactions with the -NH_2 groups of urea molecules are made possible by the polar carbonyl and amide groups of PVP, which also serve as strong hydrogen-bond acceptors and promote strong interactions with TiO_2 nanoparticles. This leads to localized enrichment of urea at the polymer-coated interface, enhancing surface wettability, electrolyte accessibility, and interfacial charge transfer [60].

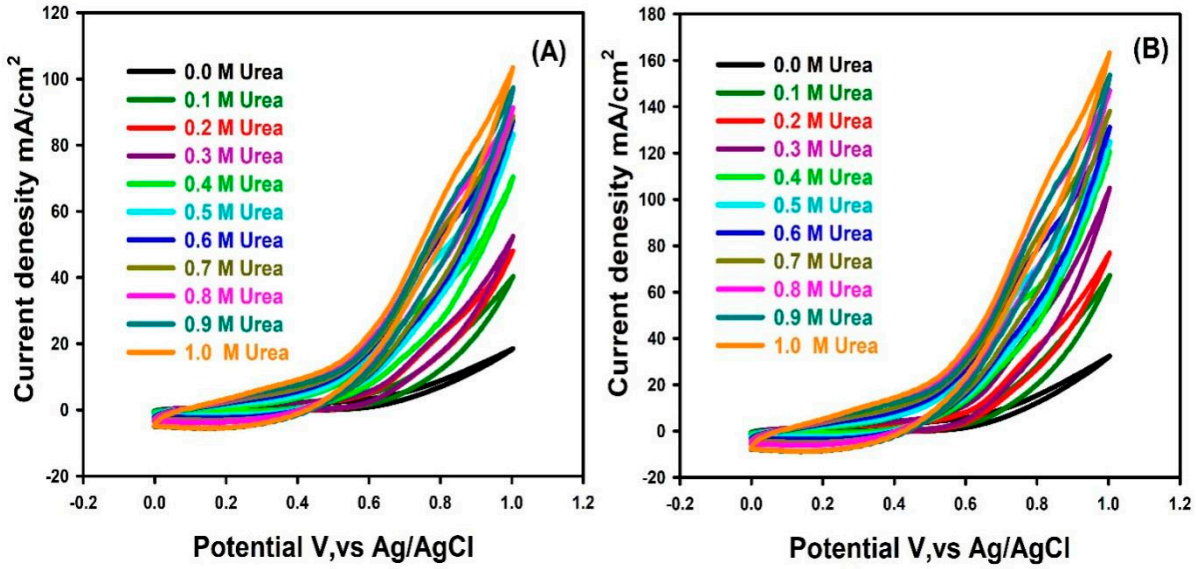

Figure 11. CV curves for (**A**) TiO_2–AC and (**B**) TiO_2–AC/PVP recorded at concentrations ranging from 0 to 1 M urea.

Effects of Different Scan Rates

The influence of the scan rate on the electrochemical performance of TiO_2–AC was investigated before and after PVP adsorption. Prior to adsorption, the current response of the TiO_2-AC electrode proportionally increased with increasing scan rate, indicating efficient charge transfer and strong electrochemical activity at the electrode interface (Figure 12A). The cyclic voltammograms maintained consistent shapes across scan rates, reflecting stable reaction kinetics and dependable performance [61]. The peak current density and the square root of the potential scan rate are shown in Figure 12C. The anodic peak intensities

increased in a direction that was proportional to the square root of the potential scan rate. In two samples, straight lines with a correlation factor near unity were produced. This demonstrates that urea or its intermediates diffuse into the pores of the samples [36]. Compared with the other nanocomposites, TiO_2-AC/PVP has a larger line slope. This slope variation indicates increased activity and is linked to a change in electrocatalytic ability [36]. The slope becomes steeper with increasing dispersion [62]. These results suggest that the oxidation process is governed by diffusion mechanisms. With increasing scan rate, the increase in oxidation manifests as an increase in the oxidation current density [63].

Linear Sweep Voltammetry

While still enabling quantitative evaluation and identification of redox processes, linear sweep voltammetry (LSV) provides a straightforward and frequently simpler method for investigating the kinetics and mechanisms of electrochemical reactions [64]. The TiO_2–AC composite performs extremely well in urea electrooxidation, as shown in Figure 13A, reaching a maximum current density of 103.4 mA/cm^2. On the other hand, TiO_2–AC/PVP achieves a current density of 163.2 mA/cm^2. The variances in the LSV profiles of the materials, which are impacted by conditions such as surface properties, catalyst amount, and structural features, clearly reveal these variations in catalytic activity. As an effective and promising electrocatalyst for urea oxidation, the TiO_2–AC/PVP sample exhibited favorable catalytic characteristics.

The relationship between the overpotential and current density is described by the Tafel slope, which offers more information about the kinetics of the reaction. It is calculated by fitting the Tafel region of the polarization curve obtained from the LSV data with a straight line [65,66]. The Tafel plot makes it possible to calculate the overpotential needed for driving the urea oxidation reaction to a particular current density. The Tafel curves for each synthetic sample at the ideal urea concentration are shown in Figure 13B. The overpotential values were computed from potentials measured vs. Ag/AgCl. Using the conventional relationship, the relevant conversion to the reversible hydrogen electrode (RHE) (Equation (1)). The extra potential required to cross the reaction's activation energy barrier is represented by the overpotential, which is defined as the difference between the applied potential and the equilibrium potential. Improving the effectiveness of urea electrooxidation requires lowering this overpotential. The sample slopes obtained from the Tafel plots show that TiO_2–AC/PVP has more catalytic activity with a low voltage needed for the electrooxidation of urea (403 mV/dec) than TiO_2-AC does (420 mv/dec).

$$E_{RHE} = E_{Ag/AgCl} + 0.197 + 0.059\ pH \quad (1)$$

Stability

Chronopotentiometry tests at a constant potential of 1 V for 3600 s were conducted to assess the long-term electrochemical stability and durability of the two tested sample composites during urea oxidation in a solution of 1 M KOH and 1 M urea (Figure 14). The samples exhibited stable performance during the test, with current responses remaining consistently steady, indicating that the structural and electrochemical integrity of the composites was preserved under extended polarization. The TiO_2–AC/PVP composite demonstrated a greater and more sustained current response over time, indicating superior catalytic stability. In contrast, the current density of TiO_2–AC rapidly decreased. These findings underscore the detrimental effect of PVP on the electrochemical performance of the electrode owing to its porous nanosheet structure and robust contact between TiO_2–AC and PVP, which enhances sustained electron and mass transport.

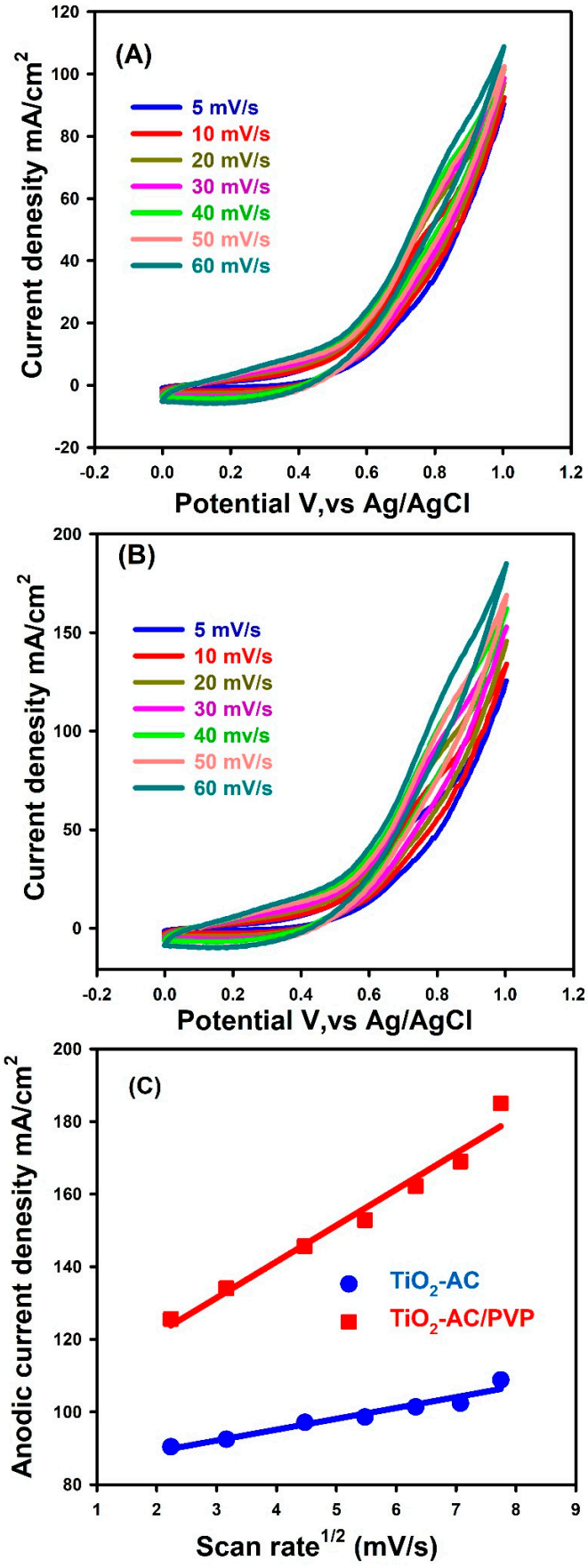

Figure 12. CV curves of the scan rate for (**A**) TiO_2–AC, (**B**) TiO_2–AC/PVP, and (**C**) the relationship between the peak current density and the square root of the scan rate.

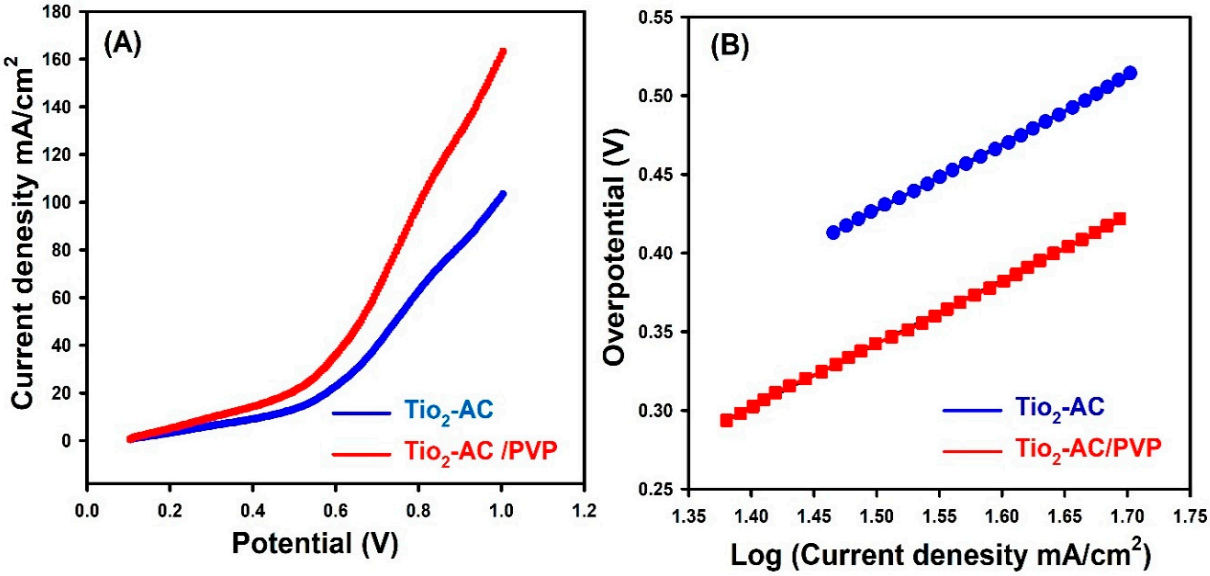

Figure 13. (**A**) Linear sweep voltammetry and (**B**) Tafel plots for the samples prepared with 1 M urea.

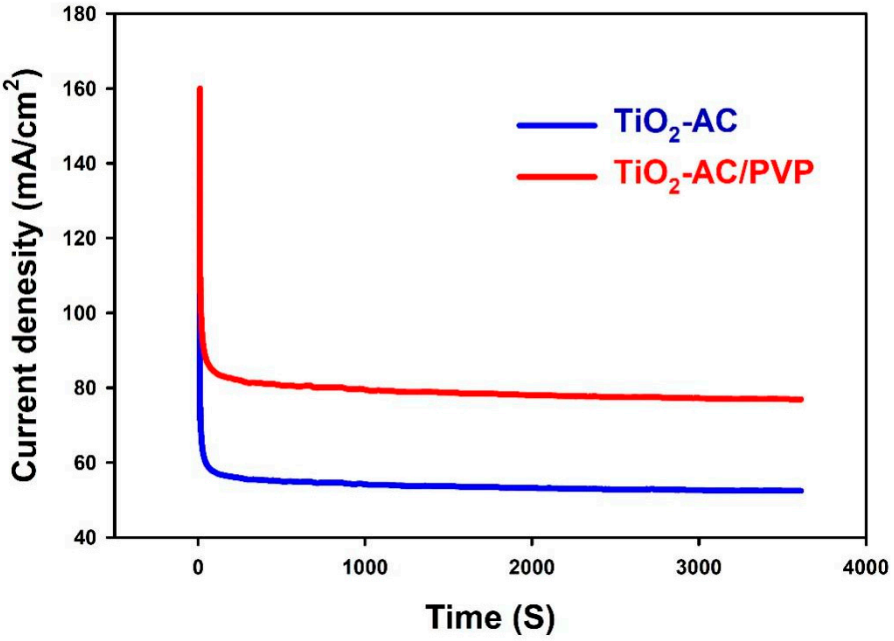

Figure 14. Chronoamperometric measurements of the prepared samples over 1 h.

2.8. Study Limitations and Future Perspectives

While this study successfully demonstrated the efficacy of the TiO_2/AC composite for the solar-driven mineralization of PVP, it is important to acknowledge its limitations in properly contextualizing the findings. These limitations, in turn, provide a clear foundation for future investigative work.

Study Limitations

The primary limitation of this work lies in its validation under controlled laboratory conditions. The performance was assessed via the use of deionized water and a single-pollutant system, but its efficacy in complex, real-world wastewater matrices that contain natural organic matter, inorganic ions, and competing contaminants that can scavenge radicals or foul the catalyst surface has not been confirmed. Furthermore, while the use of natural sunlight is a key advantage for sustainability, it introduces inherent variability in

irradiance and spectral composition, which could affect the reproducibility and predictability of degradation rates across different geographical locations and seasons. Although the TOC analysis confirmed significant mineralization, the study did not perform a detailed identification of the transient degradation intermediates and byproducts, which is crucial for a comprehensive environmental risk assessment. Finally, the ethanol regeneration protocol, although effective, involves an energy input for drying, and a full life-cycle assessment is required to evaluate the net environmental footprint of this regeneration step against the benefits of catalyst reuse.

2.9. Sustainability Assessment

The concept of green analytical chemistry (GAC) emerged to ensure that analytical chemists consider environmental, health, and safety issues during their activities. The fundamental goal is to achieve an essential balance between delivering high-quality analytical results and minimizing the environmental and health hazards associated with the analytical methods used. Since the "greenness" of analytical procedures is a multivariate and complex parameter that is not easily quantifiable, dedicated metric tools have been developed to measure the degree of sustainability in analytical methodologies. Among the key tools proposed for assessing analytical greenness and overall sustainability, three prominent methodologies stand out: the analytical eco-scale assessment (ESA), the analytical method volume intensity (AMVI), and the white analytical chemistry (WAC) approach, which are often associated with the RGB-12 algorithm.

The eco-scale score is the initially stated method [67]. The eco-scale scores are shown in Table 4.

Table 4. The penalty points of the proposed method for the analytical Eco-Scale method.

Parameters	Various Factors	Analytical Eco-Scale (AES)	Penalty Points (PP)
Toxicity	Ethanol Various Buffers	25	−10
Power	FTIR $\leq$ 1.5 Kwh-1 Potentiostat	25	0
Waste	Amounts	25	−10
Safety	Persons Instruments	25	−10
Total Points		100	−20
Eco-Scale Score		80	

The total penalty points (depending on toxicity, reagents, power, and waste) were subtracted from 100. The analytical eco-scale depends on giving penalty points to any element that does not coincide with green analysis. The penalty points concerning different parameters in the developed analytical method (the used reagents and instruments) are calculated; then, the summation of these penalty points is subtracted from 100 to obtain the eco-scale score. A method is considered an ideal ecological method if it has an eco-scale score of 100, excellent if the score exceeds 75, acceptable if it is more than 50, and inappropriate if it is less than 50 [68]. Therefore, the researcher can measure whether the method is ideally green or acceptable. A technique is considered a superior green analysis if the eco-scale score exceeds 75. The procedure will be more environmentally friendly as the score approaches 100. The new method can be seen as a green method because it points to a score of 80.

Similarly, AMVI is a method that is based on measuring the total consumed volume of solvent and the waste created from the proposed method.

The AMVI for the proposed method was calculated and was found to be 60.00% (Table 5), ensuring that this method has a limited negative impact on both human health and the environment. Generally, the eco-scale is considered more reliable than AMVI is because of its inclusiveness, consideration of solvent toxicity, and provision of a final score for the entire analytical process rather than for each individual component.

Table 5. AMVI calculation of the proposed method.

Parameters	Developed Method
Solvent consumption method (mL)	20
Volume Solvent consumption method (mL)	10
No. of full analysis	1
No. of potential analytes	1
Solvent consumption sample preparation (mL)	60
volume Standard prep. volume (mL)	10
No. of standard preps	2
volume Solvent consumption sample prep. (mL)	40
No. of Sample preps.	1
Total method solvent consumption (mL)	60
Analytical method volume intensity	60%
% Consumption method	33.3

The concept of white analytical chemistry (WAC) emerged as a proposal to reconcile the principles of green analytical chemistry with the necessary aspects of method functionality, quality, and practicality. WAC adopts a holistic vision for sustainability, recognizing that GAC tools traditionally focus mainly on environmental aspects while sometimes overlooking crucial factors such as analytical performance and economic efficiency [69].

WAC is based on the red–green–blue (RGB) additive color model, where the combination of the three primary colors ideally results in "whiteness," symbolizing a complete and well-balanced analytical methodology. The RGB-12 algorithm is the specific tool used to quantify WAC compliance, resulting in a quantitative parameter called "whiteness". This approach ensures that all attributes are treated equally to maintain the idea of sustainability, leading to a global assessment that avoids an unconditional increase in greenness at the expense of functionality [70]. The WAC approach integrates 12 WAC principles, which are divided across three complementary areas:

Red (R): Analytical efficiency/performance: This pillar includes classical validation criteria, such as the scope of application (e.g., number of analytes determined simultaneously and linearity range), limits of detection and quantification (LOD and LOQ), precision, and accuracy.

Green (G): Environmental friendliness and safety: This pillar encompasses traditional GAC concerns, including the toxicity of reagents, the number and amount of reagents and waste generated, energy consumption, and direct impacts (on humans, animals, and genetic naturalness).

Blue (B): Practical and economic aspects: This pillar reflects productivity and utility, covering cost efficiency, time efficiency, practical requirements (e.g., sample size, equipment needs, personnel qualifications), and operational simplicity (miniaturization, integration, automation, and portability).

By applying the RGB12 algorithm, a comprehensive quantitative assessment of the overall sustainability of our analytical procedures was performed, allowing for a detailed evaluation of the whiteness profile of the proposed techniques. As illustrated in Figure 15,

the methods recommended in this study achieved a notable whiteness score of 76.0. This result underscores the improved reliability, performance, and economic viability of our analytical approach.

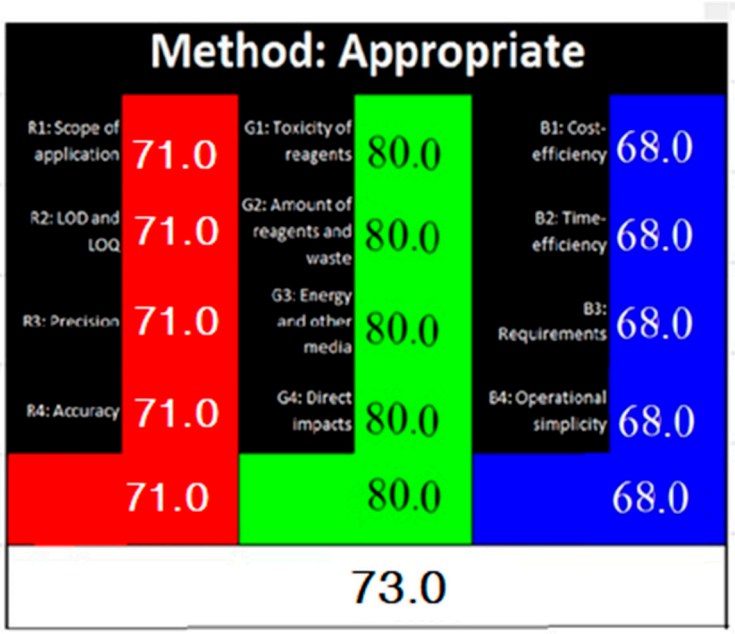

Figure 15. RGB-12 whiteness method.

2.10. Study Limitations and Future Perspectives

2.10.1. Study Limitations

While this study demonstrates effective PVP mineralization under natural sunlight, several limitations should be acknowledged. Performance was evaluated in controlled laboratory conditions using deionized water; real wastewater matrices may present additional challenges from radical scavengers or fouling agents. Although TOC analysis confirmed significant mineralization (72.1%), the specific degradation intermediates and reactive oxygen species involved were not directly identified. The proposed degradation pathway therefore remains inferential, based on the observed mineralization and general photocatalytic principles rather than system-specific radical verification. The use of natural sunlight, while sustainable, introduces irradiance variability that could affect reproducibility across locations and seasons. Finally, although the ethanol regeneration protocol is effective, a full life-cycle assessment would be needed to evaluate its net environmental footprint.

2.10.2. Future Perspectives

Building on these findings, future work should: (1) test composite performance in real industrial or municipal wastewater; (2) employ advanced characterization techniques (EPR spectroscopy, LC-MS) to definitively identify reactive species and intermediate compounds, thereby providing direct evidence for the degradation mechanism; (3) develop continuous-flow photoreactor designs for scalability; and (4) explore doping or heterojunction engineering to extend light absorption into the visible spectrum. The integrated remediation-valorization strategy presented here could also be adapted for other persistent water-soluble polymers or emerging contaminants.

3. Materials and Methods

3.1. Materials and Reagents

Polyvinylpyrrolidone (PVP K30, with an average molecular weight of approximately 40,000 Da) and hydroxy ethyl cellulose (HEC, product number 434965), with an average

Mw of 90,000, were procured from Sigma–Aldrich St. Louis, MO, USA. Titanium dioxide in the anatase crystalline phase with a purity greater than 99% was obtained from Alfa Aesar (Thermo Fisher Scientific, Waltham, MA, USA). The specific surface areas of the as-received TiO_2 and AC were approximately 48.5 m^2/g and 385.7 m^2/g, respectively. Absolute ethanol (95%) of analytical grade, used for catalyst regeneration studies, was purchased from Merck KGaA, Darmstadt, Germany. All aqueous solutions were prepared via the use of deionized water with a resistivity of 18.2 MΩ·cm produced by a Milli-Q water purification system.

3.2. Synthesis of Activated Carbon from Hydroxymethylcellulose

A measured quantity of HEC was dispersed in 180 mL of water and thermally treated at 250 °C for 8 h. After cooling to room temperature, the solid product was repeatedly washed with deionized water and ethanol and then oven-dried at 80 °C for 6 h. For activation, 1 g of the obtained carbon was placed in a closed crucible and heated in a muffle furnace at 900 °C for 1 h.

3.3. Preparation of the TiO_2/Activated Carbon Composite

The TiO_2/AC composite was prepared via a straightforward physical dry-mixing technique. This method was selected over more complex in situ synthesis routes (e.g., sol–gel) because of its scalability, reproducibility, and ability to prevent potential pore blockage of the AC support during TiO_2 nucleation. To determine the optimal composition, preliminary screening experiments were conducted by evaluating composites with TiO_2:AC mass ratios of 1:2, 1:1, 2:1, and 3:1 for their PVP adsorption capacity and subsequent photocatalytic performance under simulated sunlight. The 2:1 (w/w) ratio demonstrated the best synergistic performance, achieving an optimal balance between the photocatalytic activity of TiO_2 and the adsorptive capacity of the AC matrix. Consequently, this ratio was selected for all subsequent studies. The masses of the two components were combined in an agate mortar and blended meticulously via a pestle for 20 min to ensure a homogeneous, intimate mixture. This process was conducted to ensure the formation of a homogeneous, intimate mixture, as evidenced by a consistent gray–black coloration throughout the powder. The final composite was stored in amber glass containers to shield it from ambient light and moisture, thereby preventing any preactivation or contamination prior to use.

3.4. Experimental Design and Methodology

3.4.1. Adsorption Experiments and Parameter Optimization

The adsorption characteristics of PVP K30 onto the TiO_2/AC composite were systematically investigated through comprehensive batch experiments. All the adsorption studies were conducted in 250 mL Pyrex beakers containing 100 mL of PVP solution, with continuous agitation maintained at 300 rpm via a magnetic stirrer. The experimental design included multiple parameters to establish optimal adsorption conditions and understand the underlying mechanisms.

The effect of the pH of the solution was investigated across a range from 2–10, whereas the effect of the adsorbent dosage was evaluated across a range from 0.05 g to 0.3 g per 100 mL of PVP solution, with the initial concentration fixed at 100 mg L^{-1}. This investigation aimed to determine the relationship between catalyst mass and adsorption efficiency while identifying the optimal dosage for subsequent experiments. The influence of the initial PVP concentration was examined over an extensive range from 5 to 500 mg L^{-1}, maintaining a constant adsorbent dose of 0.2 g per 100 mL solution. Adsorption isotherm models: The equilibrium adsorption data obtained from these concentration studies were fitted to various isotherm models to comprehensively understand the adsorption mechanism, including two-parameter (Langmuir, Freundlich), three-parameter (Redlich-Peterson, Sips), four-parameter (Baudu), and five-parameter (Fritz-Schlünder) models. This broad

concentration spectrum enabled thorough analysis of the adsorption capacity and efficiency under varying pollutant loading conditions.

Kinetic studies were performed with regular sampling intervals from 0 to 24 h to capture the complete adsorption profile, including initial rapid adsorption phases and eventual equilibrium establishment. The kinetics of this adsorption process were analyzed via several models, including pseudo-first-order, pseudo-second-order, mixed 1-, 2-order, and Avrami-order models, to elucidate the underlying adsorption mechanisms and rate-controlling steps. The effect of the solution pH was critically investigated across a range of 2–9, adjusted using 0.1 M NaOH or HCl solutions, to understand the electrostatic interactions between the adsorbent surface and PVP molecules. All the adsorption experiments were conducted in complete darkness to prevent any photocatalytic interference, with the temperature maintained at 25 ± 1 °C throughout the studies. The removal efficiency (R%) and adsorption capacity (q_e, mg/g) were calculated via Equations (2) and (3):

$$R\ \% \ = \frac{C_0 - C_e}{C_0} \times 100 \tag{2}$$

$$q_e \ = \frac{(C_0 - C_e)}{m} \times V. \tag{3}$$

where C_0 and C_e represent the initial and equilibrium concentrations (mg/L), V represents the solution volume (L), and m represents the adsorbent mass (g).

3.4.2. Photocatalytic Degradation Experiments

Following the adsorption optimization studies, photocatalytic degradation experiments were performed under natural sunlight conditions. The experimental setup utilized 250 mL Pyrex reactors containing 100 mL of PVP solution with optimized parameters determined from adsorption studies: 0.2 g composite dose, initial PVP concentration of 100 mg L^{-1}, and natural pH conditions (pH 6.0).

The photocatalytic process followed a sequential methodology beginning with an 8-h adsorption phase in complete darkness to establish adsorption–desorption equilibrium. The photocatalytic phase was subsequently initiated by exposing the reaction vessels to natural sunlight. All photocatalytic experiments were conducted under natural sunlight to assess practical utility and sustainability. The experiments were performed during the summer months (June–August) in Cairo, Egypt, between 10:00 AM and 4:00 PM to capitalize on peak irradiance. Solar irradiance was monitored throughout the experiments via a calibrated Kipp & Zonen CMP6 pyranometer, with measured intensities ranging between 900 and 1000 W m^{-2}. To account for the inherent variability of natural sunlight (e.g., due to transient cloud cover or atmospheric conditions), the experiments for each data point, including the full 48-h kinetic profile, were repeated in triplicate on different days, and the results are reported as the mean values ± standard deviations. This approach ensures that the reported performance reflects a robust average under realistic, fluctuating solar conditions.

Control experiments were designed to validate the photocatalytic mechanism, including photolytic degradation, where PVP solutions without catalyst were exposed to identical solar irradiation conditions to quantify direct photolysis effects; dark adsorption, where composite-containing solutions were maintained in darkness throughout the experimental duration to assess the adsorption contribution; component evaluation, where the individual performances of pure TiO_2 and activated carbon were evaluated separately under identical conditions; and finally, catalyst regeneration, where multiple cycles were performed using ethanol-regenerated composite to assess stability and reusability.

Aliquots of the reaction mixture were systematically withdrawn at predetermined temporal intervals (0, 2, 4, 6, 8, 12, 24, 36, and 48 h) and promptly filtered through 0.45 μm membrane filters to remove catalyst particulates, and the resulting filtrates were analyzed for residual PVP concentration via high-performance liquid chromatography (HPLC) and mineralization extent via total organic carbon (TOC) analysis. All the experiments were conducted in triplicate to ensure statistical significance, and the results are expressed as the means ± standard deviations.

3.4.3. Anti-Interference Performance in Simulated Wastewater

To evaluate the practical application potential of the TiO_2/AC composite, photocatalytic degradation experiments were conducted in simulated wastewater systems containing various interfering substances commonly found in industrial and domestic wastewater. Three types of simulated wastewater were prepared:

(1) Inorganic ion matrix (IIM): Deionized water containing PVP (20 mg L^{-1}) and a mixture of inorganic ions including NaCl (100 mg L^{-1}), Na_2SO_4 (50 mg L^{-1}), $NaNO_3$ (30 mg L^{-1}), $NaHCO_3$ (100 mg L^{-1}), $CaCl_2$ (50 mg L^{-1}), and $MgSO_4$ (30 mg L^{-1}). These concentrations were selected to represent typical ion levels in municipal and industrial wastewater.

(2) Natural organic matter matrix (NOMM): Deionized water containing PVP (20 mg L^{-1}) and humic acid (HA, 10 mg L^{-1}) as a representative of dissolved organic matter commonly present in natural waters and wastewater.

(3) Mixed matrix (MM): Deionized water containing PVP (20 mg L^{-1}), the inorganic ion mixture described above, and humic acid (10 mg L^{-1}), simulating a more realistic complex wastewater environment.

Control experiments were conducted in deionized water containing only PVP (20 mg L^{-1}) under identical conditions. The photocatalytic experiments followed the same procedure described in Section 3.4.2, using the optimal TiO_2/AC composite (2:1 ratio) at a catalyst loading of 1.0 g L^{-1}. The experiments were carried out under natural sunlight irradiation for 8 h following a 6-h dark adsorption period. PVP removal efficiency, TOC reduction, and apparent rate constants were determined and compared across different water matrices to assess the anti-interference capability of the composite material.

3.5. Analytical Techniques and Characterization

The synthesized materials were characterized via a variety of analytical techniques. The crystallinity and structural properties were examined via a Panalytical Empyrean X-ray diffractometer equipped with Cu-Kα radiation (λ = 0.154 nm) operating at 35 mA and 40 kV. Scanning was conducted at a rate of 8° per minute over a 2θ range of 5° to 80°. For Fourier transform infrared (FTIR) spectroscopy, 0.50 mg of each sample was mixed with 300 mg of high-purity KBr in an agate mortar, vacuum-dried for 5 min, and then pressed into a transparent light gray pellet under a pressure of 10 tons/cm^2 for 15 min. Spectral data were collected via a Bruker Vertex 70 spectrometer over a wavenumber range of 4000–400 cm^{-1}. The microstructural features of the materials were investigated via an EVO MA10 scanning electron microscope (ZEISS, Oberkochen, Germany). Elemental mapping was carried out via a Quanta FEG250-FEI scanning electron microscope (FEI, Hillsboro, OR, USA). Brunauer–Emmett–Teller (BET) analysis was performed via a TriStar II 3020 analyzer (Micromeritics, Norcross, GA, USA) to determine the surface area, pore size distribution, and specific pore volume.

The PVP concentration in the solution was measured via reverse-phase high-performance liquid chromatography (RP-HPLC). The analysis was performed with a Hi-Plex H column using an isocratic 1:1 mixture of 70% perchloric acid (pH ~1.5) and

acetonitrile at 1.5 mL/min flow, 25 °C, with detection at 210 nm and a 12-min run time [71]. The extent of PVP mineralization was directly assessed by measuring the total organic carbon (TOC) content of the filtered solutions via a TOC-L series analyzer (Shimadzu, Kyoto, Japan). The percentage mineralization was calculated on the basis of the reduction in TOC relative to the initial value according to Equation (4):

$$Mineralization\ (\%) = \frac{TOC_0 - TOC_t}{TOC_0} \times 100 \quad (4)$$

where TOC_0 is the initial total organic carbon concentration (mg/L) and TOC_t is the total organic carbon concentration after irradiation time t (mg/L).

3.6. Catalyst Regeneration and Reusability Studies

To assess the long-term stability and practical reusability of the TiO_2/AC composite, a regeneration study was performed over multiple cycles using 0.2 g of catalyst. Upon completion of a standard 48-h adsorption–photocatalysis run, the spent catalyst was recovered from the reaction mixture via centrifugation. The recovered solid was subjected to a washing procedure with 50 mL of absolute ethanol under magnetic stirring for 1 h to desorb any residual PVP and its degradation intermediates. The washed catalyst was then separated by centrifugation and dried in an oven at 80 °C for 2 h. This regenerated catalyst was subsequently employed in a new cycle of adsorption and photocatalysis under identical conditions, maintaining the 0.2 g catalyst dose throughout all five cycles to evaluate the consistency of the photocatalytic performance.

3.7. Fabrication of the Working Electrode

The working electrode was prepared by dispersing 5.0 mg of the spent adsorbent previously employed in adsorption experiments into a solvent mixture containing 380 µL of isopropanol and 20 µL of a 4.0 wt% Nafion solution. The suspension was subjected to ultrasonic agitation for 20 min to achieve a homogeneous dispersion and reduce particle agglomeration, both of which are critical for consistent electrochemical performance. Following sonication, 20 µL of the resulting suspension was drop-cast onto a precut piece of graphite paper (1 cm × 1 cm, thickness: 1.5 mm). The electrode was then left to air dry at room temperature, allowing solvent evaporation and the formation of a uniform and stable catalytic layer.

3.8. Electrochemical Measurements

Electrochemical characterization of the modified electrodes was performed via a Metrohm AUTOLAB PGSTAT 302 N potentiostat/galvanostat operated via NOVA 1.11 software. All measurements were conducted in a standard three-electrode system within a glass electrochemical cell at room temperature. The reference electrode was Ag/AgCl (saturated KCl), the counter electrode was a platinum wire, and the working electrode was the fabricated graphite paper modified with the spent adsorbent. The electrocatalytic activity was evaluated in 1 M KOH, both with and without urea at various concentrations, to simulate real-world electrocatalytic conditions. Cyclic voltammetry (CV) was carried out over a potential range of 0–1 V versus Ag/AgCl, with scan rates varying from 5–60 $mV \cdot s^{-1}$, to investigate the redox behavior and determine the kinetic parameters of the electrocatalytic process. Additionally, chronoamperometry (CA) was conducted at a constant potential of 1.0 V for 1 h to assess the long-term operational stability. The time-dependent current profiles obtained from CA provided insight into the catalyst's durability and practical applicability for sustained urea oxidation.

3.9. Sustainability Evaluation

The greenness of the proposed method in this work was evaluated via an array of strategies that enable a thorough evaluation from many perspectives. Among the key tools proposed for assessing analytical greenness and overall sustainability, three prominent methodologies, the analytical eco-scale assessment (ESA), the analytical method volume intensity (AMVI), and the white analytical chemistry (WAC) approach, which are often associated with the RGB-12 algorithm, are used.

4. Conclusions

This study successfully developed and validated a sustainable, solar-powered strategy for the effective adsorption and profound mineralization of the persistent water-soluble polymer polyvinylpyrrolidone (PVP). The innovative TiO_2/activated carbon (2:1) composite, fabricated via a simple and scalable physical mixing method, functions as a synergistic platform that overcomes the individual limitations of its components through a well-defined "adsorb-and-shuttle" mechanism. Under natural sunlight, the composite achieved a remarkable 86.4% removal of PVP, with the critical metric of mineralization reaching 72.1%, as rigorously confirmed by TOC analysis.

The practical applicability of the composite was substantiated through tests in simulated wastewater, where it demonstrated notable resilience. Despite the presence of common interferents such as inorganic ions and humic acid, the material retained approximately 70% PVP removal efficiency in a complex mixed matrix, underscoring its potential for real-world application. A straightforward and optimized ethanol-washing process effectively regenerated the catalyst, allowing it to retain 85% of its original efficiency over five consecutive operational cycles. A comprehensive techno-economic assessment revealed that this regeneration protocol becomes economically advantageous at industrial scales (>1000 kg catalyst/year), offering up to 63% cost savings compared to fresh catalyst use, with manageable physical loss (~1.8% per cycle) and high ethanol recovery (>92%).

Furthermore, embracing a waste-to-resource paradigm, the spent TiO_2–AC/PVP composite was innovatively repurposed as a low-cost electrocatalyst for direct urea fuel cells. The PVP-modified composite showed significantly enhanced electrocatalytic activity, reaching 163.7 mA cm^{-2} compared to 103.4 mA cm^{-2} for the pristine material, due to improved interfacial properties and favorable urea enrichment at the catalyst surface. Finally, the environmental sustainability of the proposed method was quantitatively affirmed via ESA, AMVI, and RGB-12 (WAC) assessment tools.

In conclusion, this work establishes a solar-driven, circular-economy strategy that seamlessly couples the efficient remediation of a recalcitrant water-soluble pollutant with the subsequent valorization of the spent adsorbent into a valuable energy catalyst. This integrated approach offers a promising pathway for sustainable water treatment and resource recovery.

Supplementary Materials: The following supporting information can be downloaded at: https://www.mdpi.com/article/10.3390/catal16030213/s1, Figure S1: Effect of inorganic ions on PVP degradation and mineralization under sunlight irradiation. (a) PVP removal efficiency in deionized water (DI) and inorganic ion matrix (IIM) after 8 h of irradiation; (b) corresponding TOC mineralization efficiency; (c) apparent rate constant (k_{app}) for PVP degradation under different water matrices; Figure S2: Effect of natural organic matter (NOM) on PVP degradation and mineralization under solar irradiation. (a) PVP removal efficiency in deionized water and NOM matrix (NOMM) containing humic acid (HA) after 8 h of irradiation; (b) corresponding TOC mineralization efficiency; Figure S3. Photocatalytic performance in mixed-matrix simulated wastewater (MM). (a) PVP removal efficiency and (b) TOC mineralization efficiency in deionized water and mixed-matrix (MM) systems after 8 h of solar irradiation; Table S1. Isotherm model parameters for the adsorption of PVP onto the

TiO_2/AC composite; Table S2. Statistical parameters of the isotherm model for the adsorption of PVP onto the TiO_2/AC composite; Table S3. Parameters of the kinetic models for the adsorption of PVP onto the TiO_2/AC composite; Table S4. Regeneration parameter optimization data for the TiO_2/AC composite; Table S5. Ethanol recovery and catalyst mass loss over five regeneration cycles; Table S6. Projected cost comparison for catalyst regeneration across operational scales.

Author Contributions: S.M.M.: Conceptualization, Methodology, Investigation, Writing—original draft; H.A.S.: Resources, Methodology, Funding; A.A.A.: Data curation, Funding, Visualization; A.M.R.: Material synthesis, Characterization (FTIR, XRD, SEM, TEM), Data interpretation; H.N.H.E.: Investigation, Analytical validation, Real sample analysis; H.M.: Validation, Writing—review & editing; R.M.: Conceptualization, Supervision, Project administration, Data interpretation, Writing—review & editing. All authors have read and agreed to the published version of the manuscript.

Funding: This work was supported and funded by the Deanship of Scientific Research at Imam Mohammad Ibn Saud Islamic University (IMSIU) (grant number IMSIU-DDRSP2601).

Institutional Review Board Statement: Not applicable, as the study did not apply to human or animal studies. The article does not include any studies on human participants or animals conducted by any of the authors.

Data Availability Statement: The datasets generated and/or analyzed during this study are available from the corresponding author upon reasonable request.

Conflicts of Interest: The authors declare no conflicts of interest.

References

1. Franco, P.; De Marco, I. The Use of Poly (N-vinyl pyrrolidone) in the Delivery of Drugs: A Review. *Polymers* **2020**, *12*, 1114.
2. Mikayilov, E.; Tagiyev, D.; Zeynalov, N.; Tagiyev, S. Exploring the Role of Poly (N-vinyl pyrrolidone) in Drug Delivery. *Chem. Biochem. Eng. Q.* **2024**, *38*, 185–196. [CrossRef]
3. Tarring, E.C.; Robison-Smith, C.; Ceballos-Ramirez, A.D.; Durance, I.; Harbottle, M.J.; Cable, J.; Ward, B.D. Toxicity of the water-soluble polymer PVP is dependent on molecular weight and feed concentration for a freshwater model species. *Sci. Total Environ.* **2025**, *983*, 179686. [CrossRef]
4. El-Houssiny, A.S.; Ward, A.A.M.; Mansour, S.H.; Abd-El-Messieh, S.L. Biodegradable blends based on polyvinyl pyrrolidone for insulation purposes. *J. Appl. Polym. Sci.* **2012**, *124*, 3879–3891. [CrossRef]
5. Pu, H.; Du, Y.; Xia, X.; Ye, H.; Li, X.; Li, Q.; Yang, C.; Chen, L.; Tang, D. Enhanced photocatalytic performance of titanium dioxides by modulating defect contents and carbon deposits through a simple gas–solid interface reaction. *New J. Chem.* **2025**, *49*, 11729–11737. [CrossRef]
6. Nagaraj, K.; Radha, S.; Deepa, C.G.; Raja, K.; Umapathy, V.; Badgujar, N.P.; Parekh, N.M.; Manimegalai, T.; Devi, L.A.; Uthra, C. Photocatalytic advancements and applications of titanium dioxide (TiO_2): Progress in biomedical, environmental, and energy sustainability. *Next Res.* **2025**, *2*, 100180. [CrossRef]
7. Liu, W.; Wang, B.; Zhang, M. Effect of Process Parameters on the Microstructure and Performance of TiO_2-Loaded Activated Carbon. *ACS Omega* **2021**, *6*, 35076–35092. [CrossRef] [PubMed]
8. Yue, Y.; Yue, X.; Tang, X.; Han, L.; Wang, J.; Wang, S.; Du, C. Synergistic adsorption and photocatalysis study of TiO_2 and activated carbon composite. *Heliyon* **2024**, *10*, e30817. [CrossRef]
9. Safri, A.; Fletcher, A.J. Effective Carbon/TiO_2 Gel for Enhanced Adsorption and Demonstrable Visible Light Driven Photocatalytic Performance. *Gels* **2022**, *8*, 215. [CrossRef]
10. Parvathiraja, C.; Katheria, S.; Siddiqui, M.R.; Wabaidur, S.M.; Islam, M.A.; Lai, W.-C. Activated carbon-loaded titanium dioxide nanoparticles and their photocatalytic and antibacterial investigations. *Catalysts* **2022**, *12*, 834. [CrossRef]
11. Chobchun, M.; Jutakridsada, P.; Thiamsinsangwon, P.; Kasemsiri, P.; Kamwilaisak, K.; Chindaprasirt, P. Characterization of TiO_2-activated carbon onto adsorption and photocatalytic properties and its application. *J. Met. Mater. Miner.* **2020**, *30*, 30–38. [CrossRef]
12. Zhang, J.-Y.; Boyd, I.W.; O'sullivan, B.J.; Hurley, P.K.; Kelly, P.V.; Senateur, J.-P. Nanocrystalline TiO_2 films studied by optical, XRD and FTIR spectroscopy. *J. Non. Cryst. Solids* **2002**, *303*, 134–138. [CrossRef]
13. Kumar, P.M.; Badrinarayanan, S.; Sastry, M. Nanocrystalline TiO_2 studied by optical, FTIR and X-ray photoelectron spectroscopy: Correlation to presence of surface states. *Thin Solid. Films* **2000**, *358*, 122–130. [CrossRef]
14. Ali, R.; Aslam, Z.; Shawabkeh, R.A.; Asghar, A.; Hussein, I.A. BET, FTIR, and RAMAN characterizations of activated carbon from waste oil fly ash. *Turk. J. Chem.* **2020**, *44*, 279–295.

15. Mateo, W.; Lei, H.; Villota, E.; Qian, M.; Zhao, Y.; Huo, E.; Zhang, Q.; Lin, X.; Wang, C.; Huang, Z. Synthesis and characterization of sulfonated activated carbon as a catalyst for bio-jet fuel production from biomass and waste plastics. *Bioresour. Technol.* **2020**, *297*, 122411. [CrossRef] [PubMed]
16. Subramani, A.K.; Byrappa, K.; Kumaraswamy, G.N.; Ravikumar, H.B.; Ranganathaiah, C.; Rai, K.M.L.; Ananda, S.; Yoshimura, M. Hydrothermal preparation and characterization of TiO_2: AC composites. *Mater. Lett.* **2007**, *61*, 4828–4831.
17. Anjali, K.K.; Sivakumar, M. Optical absorption enhancement of PVP capped TiO_2 nanostructures in the visible region. *Solid State Ion.* **2019**, *337*, 33–41.
18. Zhou, C.; Sun, Y.; Zhang, F.; Wu, Y. Degradation of Minocycline by the Adsorption-Catalysis Multifunctional PVDF-PVP-TiO_2 Membrane: Degradation Kinetics, Photocatalytic Efficiency, and Toxicity of Products. *Int. J. Environ. Res. Public Health* **2021**, *18*, 12339. [CrossRef]
19. Gong, Y.; Wang, H.; Wei, Z.; Xie, L.; Wang, Y. An efficient way to introduce hierarchical structure into biomass-based hydrothermal carbonaceous materials. *ACS Sustain. Chem. Eng.* **2014**, *2*, 2435–2441. [CrossRef]
20. Mahgoub, S.M.; Shehata, M.R.; Zaher, A.; El-Ela, F.I.A.; Farghali, A.; Amin, R.M.; Mahmoud, R. Cellulose-based activated carbon/layered double hydroxide for efficient removal of Clarithromycin residues and efficient role in the treatment of stomach ulcers and acidity problems. *Int. J. Biol. Macromol.* **2022**, *215*, 705–728. [CrossRef] [PubMed]
21. Sutisna, S.; Rokhmawati, I.E.N.; Misto, M.; Rofi'i, I.; Mulyono, T.; Siswanto, S.; Supriyanto, E.; Wibowo, E. One step synthesis of TiO_2-activated carbon composite using hydrothermal method with mass variation of activated carbon. *Positron* **2023**, *13*, 21–30. [CrossRef]
22. Le, P.H.; Vy, T.T.T.; Van Thanh, V.; Hieu, D.H.; Tran, Q.-T.; Nguyen, N.-V.T.; Uyen, N.N.; Tram, N.T.T.; Toan, N.C.; Xuan, L.T. Facile and economical preparation method of TiO_2/activated carbon for photocatalytic degradation of methylene blue. *Micromachines* **2024**, *15*, 714. [CrossRef]
23. Abdelwahab, A.; Alenezi, K.M.; Humaidi, J.R.; Haque, A.; Mahgoub, S.M.; Mokhtar, A.M.; Shaban, A.; Mansour, M.M.; Mahmoud, R. Innovative eco-sustainable reishi mushroom-based adsorbents for progesterone removal and agricultural sustainability. *RSC Adv.* **2025**, *15*, 16690–16707. [CrossRef]
24. Chu, L.; Qin, Z.; Yang, J.; Li, X. Anatase TiO_2 nanoparticles with exposed {001} facets for efficient dye-sensitized solar cells. *Sci. Rep.* **2015**, *5*, 12143.
25. Al-Hada, N.M.; Xu, S.; Al-Ghaili, A.M.; Al-Asbahi, B.A.; Baqiah, H.; Yang, J.; Azlan, M.N.; Li, Q. Recent advances in PVP-assisted thermal treatment: Impact on nanostructure properties, potential applications, challenges, and future perspectives. *Results Phys.* **2024**, *65*, 107990. [CrossRef]
26. Lim, T.-T.; Yap, P.-S.; Srinivasan, M.; Fane, A.G. TiO_2/AC composites for synergistic adsorption-photocatalysis processes: Present challenges and further developments for water treatment and reclamation. *Crit. Rev. Environ. Sci. Technol.* **2011**, *41*, 1173–1230. [CrossRef]
27. Wu, J.; Yi, S.; Wang, Y.; Yao, J.; Gao, W. Polymer-based TiO_2 nanocomposite membrane: Synthesis and organic pollutant removal. *Int. J. Smart Nano Mater.* **2021**, *12*, 129–145.
28. Chen, X.; Mao, S.S. Titanium dioxide nanomaterials: Synthesis, properties, modifications, applications. *Chem. Rev.* **2007**, *107*, 2891–2959. [CrossRef]
29. Py, X.; Guillot, A.; Cagnon, B. Nanomorphology of activated carbon porosity: Geometrical models confronted to experimental facts. *Carbon* **2004**, *42*, 1743–1754. [CrossRef]
30. Ayanda, O.S.; Fatoki, O.S.; Adekola, F.A.; Ximba, B.J. Activated Carbon-Fly Ash-Nanometal Oxide Composite Materials: Preparation, Characterization, and Tributyltin Removal Efficiency. *J. Chem.* **2013**, *2013*, 148129.
31. Li, Y.; Zhang, S.; Yu, Q.; Yin, W. The effects of activated carbon supports on the structure and properties of TiO_2 nanoparticles prepared by a sol–gel method. *Appl. Surf. Sci.* **2007**, *253*, 9254–9258. [CrossRef]
32. Archana, D.; Singh, B.K.; Dutta, J.; Dutta, P.K. In vivo evaluation of chitosan–PVP–titanium dioxide nanocomposite as wound dressing material. *Carbohydr. Polym.* **2013**, *95*, 530–539. [CrossRef]
33. El-Bery, H.M.; Salah, M.R.; Ahmed, S.M.; Soliman, S.A. Efficient non-metal based conducting polymers for photocatalytic hydrogen production: Comparative study between polyaniline, polypyrrole and PEDOT. *RSC Adv.* **2021**, *11*, 13229–13244. [CrossRef] [PubMed]
34. Balaji, S.; Guda, R.; Mandal, B.K.; Kasula, M.; Ubba, E.; Khan, F.-R.N. Green synthesis of nano-titania (TiO_2 NPs) utilizing aqueous Eucalyptus globulus leaf extract: Applications in the synthesis of 4 H-pyran derivatives. *Res. Chem. Intermed.* **2021**, *47*, 3919–3931. [CrossRef]
35. Jukić, J.; Juračić, T.; Josić, E.; Namjesnik, D.; Begović, T. Effects of polyion adsorption on surface properties of TiO_2. *Adsorption* **2024**, *30*, 251–264. [CrossRef]
36. Abdel-Hady, E.E.; Mahmoud, R.; Hafez, S.H.M.; Mohamed, H.F.M. Hierarchical ternary ZnCoFe layered double hydroxide as efficient adsorbent and catalyst for methanol electrooxidation. *J. Mater. Res. Technol.* **2022**, *17*, 1922–1941. [CrossRef]

37. El Kawas, N.M.; Zaki, A.H.; Taha, M. Methylene blue and methyl orange removal using green rust as a low-cost, sustainable adsorbent and photocatalyst. *RSC Adv.* **2025**, *15*, 18403–18418. [CrossRef]
38. Akıllı, A.; Özler, A.; Taymaz, B.H.; Hancı, A.; Eskizeybek, V.; Kamış, H. Adsorption-Assisted Photocatalytic Degradation of Anionic Direct Yellow-50 and Cationic Methylene Blue Dyes by Chemically Synthesized Poly(1,5-diaminoanthraquinone). *J. Inorg. Organomet. Polym. Mater.* **2025**, *35*, 5509–5530. [CrossRef]
39. Morante, N.; Monzillo, K.; Vaiano, V.; Kadirova, Z.C.; Sannino, D. Synthesis and Characterization of a Novel Sol-Gel-Derived Ni-Doped TiO_2 Photocatalyst for Rapid Visible Light-Driven Mineralization of Paracetamol. *Nanomaterials* **2025**, *15*, 530. [CrossRef]
40. Yadav, V.; Verma, P.; Negi, H.; Singh, R.K.; Saini, V.K. Efficient degradation of 4-nitrophenol using VO(TPP) impregnated TiO_2 photocatalyst: Insight into kinetics and mechanism. *J. Mater. Res.* **2023**, *38*, 237–247. [CrossRef]
41. Florez, J.; Diaz-Uribe, C.; Vallejo, W.; Duran, F.; Puello, E.; Salazar, J.; Zarate, X.; Schott, E. Study of methylene blue removal and photocatalytic degradation on zirconia thin films modified with Mn-Anderson polyoxometalates. *Dalt. Trans.* **2025**, *54*, 2471–2482. [CrossRef]
42. Du, C.; Wang, S.; Miao, X.; Sun, W.; Zhu, Y.; Wang, C.; Ma, R. Polyvinylpyrrolidone as additive for perovskite solar cells with water and isopropanol as solvents. *Beilstein J. Nanotechnol.* **2019**, *10*, 2374–2382. [CrossRef]
43. Shqier, R.; Zyoud, A.; Helal, M.H.S.; Nassar, H.; Alkowni, R.; Assali, M.; Zyoud, S.; Qamhieh, N.; Hajamohideen, A.R.; Sawalha, S. TiO_2 nanopowder and nanofilm catalysts in the disinfection and mineralization of S. aureus with solar-simulated radiation. *React. Chem. Eng.* **2024**, *9*, 1762–1775.
44. Garay-Rodríguez, L.F.; Zermeño, B.; López de la O, K.A.; Leyva, E.; Moctezuma, E. Photocatalytic degradation of Bisphenol A: Kinetic studies and determination of the reaction pathway. *J. Appl. Res. Technol.* **2018**, *16*, 334–345. [CrossRef]
45. Farghaly, A.; Maher, E.; Gad, A.; El-Bery, H. Synergistic photocatalytic degradation of methylene blue using TiO_2 composites with activated carbon and reduced graphene oxide: A kinetic and mechanistic study. *Appl. Water Sci.* **2024**, *14*, 228. [CrossRef]
46. Del Angel, R.; Durán-Álvarez, J.C.; Zanella, R. Tio_2-Low Band Gap Semiconductor Heterostructures for Water Treatment Using Sunlight-Driven Photocatalysis. In *Titanium Dioxide—Material for a Sustainable Environment*; IntechOpen: London, UK, 2018; p. 305.
47. Perović, K.; Rosa, F.M.D.; Kovačić, M.; Kušić, H.; Štangar, U.L.; Fresno, F.; Dionysiou, D.D.; Bozic, A.L. Recent Achievements in Development of TiO_2-Based Composite Photocatalytic Materials for Solar Driven Water Purification and Water Splitting. *Materials* **2020**, *13*, 1338. [CrossRef] [PubMed]
48. Ajmal, A.; Majeed, I.; Malik, R.N.; Idriss, H.; Nadeem, M.A. Principles and mechanisms of photocatalytic dye degradation on TiO_2 based photocatalysts: A comparative overview. *RSC Adv.* **2014**, *4*, 37003–37026.
49. Wang, H.; Zheng, X.; Fang, L.; Lu, S. Urea electrooxidation in alkaline environment: Fundamentals and applications. *ChemElectroChem* **2023**, *10*, e202300138. [CrossRef]
50. Schranck, A.; Marks, R.; Yates, E.; Doudrick, K. Effect of urine compounds on the electrochemical oxidation of urea using a nickel cobaltite catalyst: An electroanalytical and spectroscopic investigation. *Environ. Sci. Technol.* **2018**, *52*, 8638–8648. [CrossRef]
51. Vedharathinam, V. Electrochemical Oxidation of Urea on Nickel Catalyst in Alkaline Medium: Investigation of the Reaction Mechanism. Ph.D. Thesis, Ohio University, Athens, OH, USA, 2015.
52. Aladeemy, S.A.; Al-Mayouf, A.M.; Shaddad, M.N.; Amer, M.S.; Almutairi, N.K.; Ghanem, M.A.; Alotaibi, N.H.; Arunachalam, P. Electrooxidation of urea in alkaline solution using nickel hydroxide activated carbon paper electrodeposited from DMSO solution. *Catalysts* **2021**, *11*, 102. [CrossRef]
53. Carpenter, K.; Stuve, E.M. Electrooxidation of urea and creatinine on nickel foam-based electrocatalysts. *J. Appl. Electrochem.* **2021**, *51*, 945–957. [CrossRef]
54. Wardani, A.K.; Ariono, D.; Subagjo, S.; Wenten, I.G. Fouling tendency of PDA/PVP surface modified PP membrane. *Surf. Interfaces* **2020**, *19*, 100464. [CrossRef]
55. Barakat, N.A.M.; Sayed, Y.T.; Irfan, O.M.; Abdelaty, M.M. Synthesis of TiO_2-incorporated activated carbon as an effective Ion electrosorption material. *PLoS ONE* **2023**, *18*, e0282869. [CrossRef]
56. Ortiz, D.G.; Nouxet, M.; Maréchal, W.; Lorain, O.; Deratani, A.; Pochat-Bohatier, C. Immobilization of poly (vinyl pyrrolidone) in polysulfone membranes by radically-initiated crosslinking using potassium persulfate. *Membranes* **2022**, *12*, 664. [CrossRef]
57. Qi, P.; Jia, H.; Xu, S.; Wang, Q.; Su, G.; Yang, G.; Zhang, M.; Qu, Y.; Pei, F. Preparation and separation properties of electrospinning modified membrane with ionic liquid terminating polyimide/polyvinylpyrrolidone@ polydopamine. *Membranes* **2022**, *12*, 189. [CrossRef]
58. Elbasiony, A.M.; Madani, M.; Ghobashy, M.M.; Shaban, M.; Alharthi, S.; Al-Gahtany, S.A.; Al-Shaalan, N.H.; Boraie, W.E.; Attia, M.S.; Abaza, S.F. Tailoring optical and electrical properties of PVP-I2 complexes through gamma irradiation-induced structural defect Engineering for optoelectronic applications. *Results Chem.* **2024**, *11*, 101827. [CrossRef]
59. Nieuwland, C.; van Dam, A.N.; Bickelhaupt, F.M.; Guerra, C.F. Urea hydrogen-bond donor strengths: Bigger is not always better. *Phys. Chem. Chem. Phys.* **2025**, *27*, 4099–4108. [CrossRef]

60. Hutchins, K.M. Functional materials based on molecules with hydrogen-bonding ability: Applications to drug co-crystals and polymer complexes. *R. Soc. Open Sci.* **2018**, *5*, 180564. [CrossRef]
61. Ge, W.; Lin, L.; Wang, S.-Q.; Wang, Y.; Ma, X.; An, Q.; Zhao, L. Electrocatalytic urea oxidation: Advances in mechanistic insights, nanocatalyst design, and applications. *J. Mater. Chem. A* **2023**, *11*, 15100–15121. [CrossRef]
62. Shahrokhian, S.; Rezaee, S. Vertically standing Cu_2O nanosheets promoted flower-like PtPd nanostructures supported on reduced graphene oxide for methanol electro-oxidation. *Electrochim. Acta* **2018**, *259*, 36–47. [CrossRef]
63. Li, J.; Wang, S.; Sun, S.; Wu, X.; Zhang, B.; Feng, L. A review of hetero-structured Ni-based active catalysts for urea electrolysis. *J. Mater. Chem. A* **2022**, *10*, 9308–9326. [CrossRef]
64. Jović, B.M.; Dobrovolska, T.; Lačnjevac, U.; Krastev, I.; Jović, V.D. Characterization of electrodeposited Cd–Co alloy coatings by anodic linear sweep voltammetry. *Electrochim. Acta* **2009**, *54*, 7565–7572. [CrossRef]
65. Shinagawa, T.; Garcia-Esparza, A.T.; Takanabe, K. Insight on Tafel slopes from a microkinetic analysis of aqueous electrocatalysis for energy conversion. *Sci. Rep.* **2015**, *5*, 13801. [CrossRef]
66. Murthy, A.P.; Theerthagiri, J.; Madhavan, J. Insights on Tafel constant in the analysis of hydrogen evolution reaction. *J. Phys. Chem. C* **2018**, *122*, 23943–23949. [CrossRef]
67. Gałuszka, A.; Migaszewski, Z.M.; Konieczka, P.; Namieśnik, J. Analytical Eco-Scale for assessing the greenness of analytical procedures. *TrAC Trends Anal. Chem.* **2012**, *37*, 61–72. [CrossRef]
68. Pena-Pereira, F.; Wojnowski, W.; Tobiszewski, M. AGREE—Analytical GREEnness Metric Approach and Software. *Anal. Chem.* **2020**, *92*, 10076–10082. [CrossRef]
69. Ahmed-Anwar, A.A.; Mohamed, M.A.; Farghali, A.A.; Mahmoud, R.; Hassouna, M.E.M. Green UPLC method for estimation of ciprofloxacin, diclofenac sodium, and ibuprofen with application to pharmacokinetic study of human samples. *Sci. Rep.* **2023**, *13*, 17613. [CrossRef]
70. Nowak, P.M.; Wietecha-Posłuszny, R.; Pawliszyn, J. White Analytical Chemistry: An approach to reconcile the principles of Green Analytical Chemistry and functionality. *TrAC Trends Anal. Chem.* **2021**, *138*, 116223. [CrossRef]
71. Mahgoub, S.M.; Rudayni, H.A.; Radallada, A.M.; Younes, H.A.; Allam, A.; Mahmoud, R. A Versatile Mixed-Mode HPLC Method for Sensitive Quantification of Polyvinylpyrrolidone in Pharmaceutical, Cosmetic, and Environmental Samples with a Greenness Assessment. *J. Pharm. Innov.* **2025**, *21*, 69. [CrossRef]

Disclaimer/Publisher's Note: The statements, opinions and data contained in all publications are solely those of the individual author(s) and contributor(s) and not of MDPI and/or the editor(s). MDPI and/or the editor(s) disclaim responsibility for any injury to people or property resulting from any ideas, methods, instructions or products referred to in the content.